Nature of infrared-active phonon sidebands to internal vibrations: Spectroscopic studies of solid oxygen and nitrogen

A. P. Brodyanski,[1,4] S. A. Medvedev,[1,2] M. Vetter,[1] J. Kreutz,[1] and H. J. Jodl[1,3]
[1]*Fachbereich Physik, Universität Kaiserslautern, Erwin Schrödinger Strasse, D-67663 Kaiserslautern, Germany*
[2]*National Technical University "Kharkov Polytechnical Institute," 21, Frunze Street, 61002 Kharkov, Ukraine*
[3]*LENS, European Laboratory for Non Linear Spectroscopy, Largo E. Fermi 2, I-50125 Firenze, Italy*
[4]*IFOS, Institut für Oberflächen—und Schichtanalytik, Universität Kaiserslautern, Erwin Schrödinger Strasse, D-67663 Kaiserslautern, Germany*

(Received 13 May 2002; revised manuscript received 5 August 2002; published 30 September 2002)

The ir-active phonon sidebands to internal vibrations of oxygen and nitrogen were precisely investigated by Fourier transform infrared spectroscopy in the fundamental and first overtone spectral regions from 10 K to the boiling points at ambient pressure. We showed that an analysis of ir-active phonon sidebands yields important information on the internal vibrations of molecules in a condensed medium (solid or liquid), being complementary to Raman data on vibron frequencies. Analyzing the complete profile of these bands, we determined the band origin frequencies and explored their temperature behavior in all phases of both substances. We present unambiguous direct experimental proofs that this quality corresponds to the frequency of internal vibrations of *single* molecules. Considering solid oxygen and nitrogen as two limiting cases for simple molecular solids, we interpret this result as a strong evidence for a general fact that an ir-active phonon sideband possesses the same physical origin in pure molecular solids and in impurity centers. The key characteristics of the fundamental vibron energy zone (environmental and resonance frequency shifts) were deduced from the combined analysis of ir and Raman experimental data and their temperature behavior was explored in solid and liquid phases of oxygen and nitrogen at ambient pressure. The character of the short-range orientational order was established in the β-nitrogen based on our theoretical analysis consistent with the present experimental results. We also present the explanation of the origin of pressure-caused changes in the frequency of the Raman vibron mode of solid oxygen at low temperatures.

DOI: 10.1103/PhysRevB.66.104301 PACS number(s): 63.20.Ls, 78.30.−j

I. INTRODUCTION

A common feature of the absorption spectra of molecular crystals is a broadband (width $\sim 100\ \mathrm{cm}^{-1}$) in the fundamental region (middle ir). This band is associated with a simultaneous excitation of internal and external vibrations by one photon[1,2] (double transitions) and is now called as a phonon sideband of intramolecular vibrational transition. In case of symmetric diatomic molecules (H_2, N_2, O_2), an excitation of internal vibrations is rigorously electric-dipole forbidden as one-particle process in central-symmetric crystal phases due to symmetry. That is why the phonon sideband is the only allowed ir absorption in these solids in the fundamental spectral region. The exact profile of this ir-active band is characteristic for each substance[3–5] and is changed due to temperature.[1–6] Furthermore, it is usually clearly dissimilar in different thermodynamic phases of the same solid and, consequently, can be used as a spectroscopic fingerprint of a certain crystal structure of the substance investigated.[6]

A principal theoretical explanation of a nature of the phonon sideband structure in absorption spectra was proposed by Hochstrasser and Prasad.[7] On the basis of a general theoretical description of the exciton-phonon interaction developed by Davydov,[8] they showed that a phonon sideband profile maps an intensity-weighted density of state of lattice excitations [phonon DOS (phonon density of states)]. Therefore, one can use such kind of spectroscopic investigations to render a direct information on the shape and singularities of the complete phonon DOS that was earlier only available by inelastic neutron diffraction measurements on single crystals. To prove this general idea, spectroscopic studies were carried out.[3–5] In these analyses, the experimental profile of the phonon sideband to internal vibrations was compared to the calculated shape of the density of state of lattice excitations (including many-phonon processes).[5] The frequency of either vibron excitations at $\mathbf{k}=0$ known from Raman measurements or a maximum of defect-induced vibron peak visible in thin-film absorption spectra[3–5] was chosen as a zero-phonon line (ZPL). The agreement between the experimental and calculated profiles of the phonon sidebands was fairly good, but sometimes not completely satisfactory. These authors speculated that these fine discrepancies could originate from some modification of the shape of the phonon DOS in phonon sideband spectra by unknown but mode specific coupling between internal and external excitations. They also showed that the relative positions of the maxima in the phonon sideband ir-spectra approximately correspond to the frequencies of the peaks in Raman spectra of lattice excitations.

In theoretically oriented literature, phonon sidebands have been usually treated as a combination band formed by interaction between two different kinds of quasiparticles—delocalized internal (electronic excitons,[7] vibrons[9]) and external (phonons) excitations. However, the energy band of the internal excitations was considered as dispersionless at the concrete calculations of the intensity and frequency distribution of the phonon sidebands.[7,9,10] At the spectroscopic analysis of the shape of the phonon sidebands in different molecular solids,[2,3–6,7,11] only *one* frequency of internal excitations was also used (as ZPL).

Careful analysis of experimental data on the defect-

induced ir-active vibron peak casts doubt on such a dispersionless vibron band in real solids. Cairns and Pimentel[2] observed in spectra of α-O_2 thin films that the position of this peak is noticeably varied (about 4 cm^{-1}) with the deposition conditions. Much later on, it was shown[3,4,12] that indeed this defectinduced vibron absorption forms a relatively broad band (width approximately 8 cm^{-1}) possessing an own complicated structure. A similar great dispersion (about 6 cm^{-1}) was also determined for the vibron energy band in $^1\Delta_g(1)$ electronic-excited state in α-O_2.[13] Very recently, Gorelli *et al.*[14] measured the ir-active phonon sideband to internal vibrations in high-pressure phases of solid oxygen. Using the known frequency of either Raman-or ir-active vibron peaks as a ZPL, they tried to identify the maxima in the spectra of the phonon sideband observed with the frequencies of lattice excitations measured by other groups at these pressures. No success was achieved at all. These facts question the validity of the ZPL concept traditionally used to describe (at least semiquantitatively) a phonon sideband profile.

However, the existence of a certain frequency of internal excitations as the origin of an ir-active phonon sideband was successfully tested by analyzing the phonon sidebands to electronic excitations in both low-[13] and high-pressure [15] phases of solid oxygen. The band origin frequency (as ZPL) was found by dividing an experimental sideband profile into additive and subtractive combinations of the internal and external vibrations (Stokes and anti-Stokes components of the phonon sideband). An excellent modeling of the experimental spectra of phonon sidebands was achieved by this procedure in all phases of condensed oxygen ($p=0-6$ GPa, $T=10-300$ K). Moreover, our preliminary results also pointed to the fact that a similar situation takes place in case of phonon sidebands to intermolecular *vibrations* [for α-N_2 and α-O_2 see Fig. 2(a) and 2(b) in Ref. 13]. However, the ZPL frequency determined did not coincide with the frequency of vibron excitations well known from Raman spectra for both substances. We speculated[13] that the ZPL frequency determined by our procedure corresponds to the frequency of internal excitation of a *single* molecule in the crystal. Therefore, the concrete meaning of the ZPL frequency as well as the nature of a phonon sideband in general needs considerable clarification.

To give more insight in this general problem and to obtain unambiguous direct experimental proofs of our principal idea, we carefully investigated the phonon sidebands to internal vibrations in the fundamental and overtone spectral regions by Fourier transform infrared (FTIR) spectroscopy in all condensed phases of oxygen and nitrogen at equilibrium vapor pressure as function of temperature (10–80 K). Due to excellent optical quality of our samples (no traces of defect-induced vibron absorption were observed) and due to modern FTIR technique, we were able to analyze the *complete* sideband profile quantitatively. Noticeably, such a challenge was previously practically insolvable because a strong defect-induced vibron absorption, always presented in spectra of condensed thin films,[3–5] overlapped the relatively weak anti-Stokes part of the phonon sideband spectra.

Solid oxygen and nitrogen represent two limiting cases for simple molecular crystals. Indeed, in the nitrogen phases of interest, centers of mass of N_2 molecules are located at the points of fcc (α-N_2) and hcp (β-N_2) structures.[16] In α-N_2, molecular axes are oriented along four different body diagonals forming four simple cubic sublattices (space group $Pa3$). No long-range orientational order exists in β-N_2. However, molecular axes of nitrogen molecules are preferably localized[17] at a polar angle $\vartheta=54°-56°$ relative to the c axis of β-N_2. The crystal structure of both α- and β-N_2 is mainly stabilized by an isotropic part of the intermolecular interaction and the long-range orientational order in α-N_2 is formed by the quadrupole-quadrupole interaction.[16] Liquid nitrogen seems to be similar to common simple liquids.[18] On the contrary, oxygen molecules possess a very small quadrupole moment (the smallest value among diatomic molecules) and, consequently, the direct electrostatic interaction makes a negligible contribution to practically all properties of solid and liquid oxygen. As a result, the collinear molecular configuration appears in the orientationally ordered low-temperature α-and β-O_2 (space groups $C2/m$ and $R\bar{3}m$, respectively[19]). These phases possess the layered crystal structures explicitly stabilized by the anisotropic part of the repulsive interaction.[20] The high-temperature γ-O_2 has a cubic structure (space group $Pm3n$) characterized by two different kinds of the crystallographic positions of molecules (a and c). Two oxygen molecules, occupying a positions, possess practically spherical distribution of the electronic density (so-called ''spherelike'' (sp) molecules), whereas molecular axes of six molecules, located in c positions, are almost stochastically distributed perpendicular to $\langle 001\rangle$ directions (so-called ''disklike'' (d) molecules).[19] The isotropic part of the dispersion interaction is mainly responsible for a general stability of this ''exotic'' crystal structure.[20] Due to nonzero electronic spin ($S=1$) in the electronic ground state ($^3\Sigma_g^-$), solid oxygen combines properties of a cryocrystal and a magnet. Furthermore, α-O_2 is a two-sublattice antiferromagnet.[21] Only a short-range magnetic order exists in β- and γ-O_2.[21(b),22] Strong short-range spin-spin[15,18(b),22] and orientational[15,18(b)] correlations persist also in liquid oxygen. Therefore, a comparative analysis of these two substances—N_2 and O_2—allows us to check the generality of our idea as well as to comprehend key factors governing the behavior of vibron excitations in simple molecular crystals.

This paper is structured as follows. In the following section, we will sketch our experimental procedure paying main attention to crystal growth details that influence crucially the optical quality of the samples. Our experimental spectroscopic results together with their theoretical analysis and discussion will be presented in the following section. First, we will illustrate the applicability of our general approach to model the profile of phonon sidebands to fundamental vibrations as well as to determine the corresponding ZPL frequencies. We will compare these values to known Raman data on the vibron fundamental frequencies as well as to the isotope data and discuss possible explanations of our obtained results. Second, we will analyze phonon sidebands to vibrational overtones to clear up the physical meaning of the ZPL frequency. Third, we will deduce the key characteristics of

the fundamental energy band (environmental and resonance frequency shifts) in our substances and will explore their behavior in details including a possible scenario at high pressures. Fourth, we will clarify the peculiarities of the short-range orientational order in β-N_2 based on our theoretical analysis of spectroscopic results.

II. EXPERIMENTAL PROCEDURE

We investigated liquid and solid oxygen and nitrogen by FTIR spectroscopy in the temperature range from 10 K to boiling points at equilibrium vapor pressure (solid) and at 1.5 bars (liquid). The spectra were recorded in mid-infrared spectral region by a Fourier spectrometer (Bruker IFS 120 HR) both at cooling and at warming of the samples. The phonon sidebands to the fundamental vibrations of oxygen were measured by using the following experimental setup: a glowbar light source, a KBr beam splitter, and a liquid-N_2-cooled mercury cadmium tellurid (MCT) detector (accessible spectral range 800–5000 cm^{-1}). To precisely measure the substantially weaker phonon sidebands to fundamental vibrations of nitrogen as well as to first vibrational overtone in both substances we used a tungsten lamp as light source, Si on CaF_2 as beam splitter, and a liquid-N_2-cooled InSb detector (accessible spectral range 1900–11 000 cm^{-1}). The diameter of the diaphragm was 0.8–1.0 mm and 1.7 mm for oxygen and nitrogen samples, respectively. The frequency resolution was varied from 0.05 to 0.5 cm^{-1}, depending on the bandwidth of interest in spectra. The Raman spectra of the fundamental vibron excitations were precisely measured in solid and liquid oxygen for comparison with the ir data. The 488 nm emission of an Ar^+ laser was used as an excitation line. The Raman signal was detected by a Peltier-effect cooled multiplier. To analyze a profile of the relatively narrow vibron bands correctly we used the so-called tandem arrangement—a triple monochromator (Jobin Yvon T64000) and a Fabry-Perot-Interferometer—at these measurements. To determine absolute values of the vibron frequencies with high accuracy we used a selected emission line of the Ne-lamp possessing a frequency value close to the vibron ones as an internal standard. As a result, we achieved a frequency resolution of about 0.01 cm^{-1} and an absolute accuracy determining the vibron frequency values better than 0.02 cm^{-1}.

We used in our experiments an oxygen gas of 99.998% and nitrogen gas of 99.999% purity. The brass cells with diamond (aperture 3 mm, sample thickness 1 mm) and quartz (aperture 10 mm, sample thickness 6.7 mm) windows were used to measure phonon sidebands to fundamental and overtone vibrations in oxygen, respectively. Since the phonon sidebands in solid nitrogen are characterized by more than one order of magnitude less intensity in comparison to oxygen[13] and since we intended to analyze these weak ir-active bands quantitatively, very thick samples of solid nitrogen had to be investigated. Therefore, we specially designed a copper cell with sapphire windows (aperture 10 mm) for sample thickness of 20.5 mm. All of our samples possessed a disclike form (diameter of 10 mm). Any of these cells was mounted on the cold finger of a He-closed-cycle cryostat used to achieve low temperatures. We measured the sample temperature by a calibrated Si diode that was directly attached to the sample cell. Temperature resolution was 0.005 K at $T \leqslant 25$ K and 0.04 K at higher temperatures. An absolute accuracy of the sample temperature registration was about 0.1 K (for details see Ref. 6).

To be successful in growing big polycrystalline samples for optical investigations we followed the general principles of the single crystal growth (see, e.g., Ref. 23) and adapted these for our demands. The sample cell was evacuated up to $\sim 10^{-6}$ mbar at room temperature and purged several times by the investigated gas. After that, the empty cell was cooled down to a temperature that was a bit less than the boiling point of the substance investigated. The sample gas was liquefied at an overpressure of about 0.5 bars. To ensure a complete filling of the sample chamber as well as a good thermal contact of our solid sample with walls of the sample chamber during crystallization process this gas overpressure was maintained up to finishing the crystal growth procedure. Changes in our samples during the whole growth procedure were continuously monitored spectroscopically. After condensation, the liquid sample was cooled down (3 K/h) towards the melting point to grow slowly (0.1 K/h) the crystal. At a temperature slightly lower than the crystallization point ($\Delta T = 0.1 - 0.5$ K), the grown crystal was annealed during 10–20 h. The annealed samples were completely transparent to visible light controlled by eye (microscope) and their continuum transmission was almost equal to the one in liquid samples. The averaged cooling rate within the temperature region of high-temperature phases was about 0.5–1 K/h depending on the number of spectra measured in these phases. No significant changes in the continuum transmission of the samples were observed during this time consuming (1–3 days) cooling procedure. In the temperature range of a solid-solid phase transition, the samples were cooled substantially slowly (0.05 K/h). The phase transformation lasted about 2–3 h. Further on, we annealed the crystal of a low-temperature phase during 10–12 h either by keeping the sample at a constant temperature (43.6 K, β-O_2) or by very slow (0.02 K/h) cooling (35.5 K$\rightarrow$35.3 K, α-N_2). As a result, we obtained big polycrystalline samples of the low-temperature phases of an excellent optical quality. For example, the continuum transmission of our α-nitrogen crystal ($V = 1.6$ cm^3) was reduced to 90% of the one of the β-N_2 only. In cooling to 10 K, the typical rate of 0.2 K/h was kept. We did not observe any significant changes in the continuum transmission of our samples passing through the α-β phase transition in solid oxygen. No traces of defect induced N_2 or O_2 vibron bands were observed in our spectra.

III. RESULTS AND DISCUSSION

A. Phonon sidebands to fundamental vibrations

1. Description of spectra

In our studies, we carefully measured the ir-active phonon sidebands to fundamental vibrations on optically perfect samples in all condensed phases of oxygen and nitrogen at ambient pressure. Previously, only the Stokes part of these absorption bands was studied on *condensed* thin films of

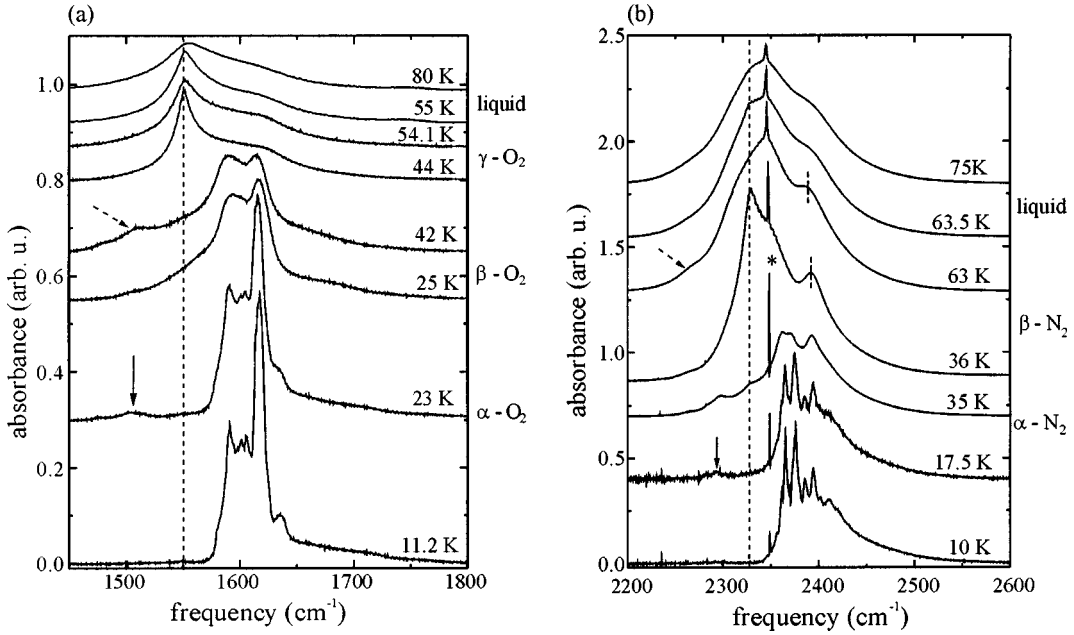

FIG. 1. Temperature evolution of absorption spectra of the phonon sideband to the fundamental vibrations in oxygen (a) and nitrogen (b). Vertical dashed lines show the position of the vibron frequency. Asterisk marks the $\nu_3 CO_2$ absorption band.

both substances up to 39 K.[4] To our knowledge, there are only two publications concerning phonon sideband spectra of γ-oxygen[1,24] and liquid phases of both substances,[1] in which only a qualitative comparison of the spectra in different phases was carried out.

The temperature evolution of the phonon sidebands of fundamental intramolecular transitions measured by us is shown in Fig. 1(a) (oxygen, sample thickness of 1 mm) and Fig. 1(b) (nitrogen, sample thickness of 20.5 mm). The frequencies of vibron modes in α-O_2 and α-N_2 (Ref. 23) are schematically shown by vertical dashed lines in Figs. 1(a) and 1(b) for comparison. Our absorption spectra were completely reproducible at cooling and warming in single-phase temperature regions. In temperature ranges of the phase transitions (solid-solid, solid-liquid), weak hysteresis phenomena were observed (0.1–0.2 K). The following general features are clearly visible in Fig. 1.

(i) At low temperatures (bottom), the spectra of both substances possess a pronounced fine structure in the frequency range corresponding to an additive combination of intramolecular and intermolecular vibrations. The maxima of this structure reflect the singularities of the phonon DOS in each substance[5,26(a)] and their assignment was already done for α- and β-oxygen[4,6,13] as well as for α-nitrogen.[4,5] As temperature increases, these maxima are continuously smeared out. Only a broad feature, whose maximum is situated at the frequency of about 2390 cm^{-1}, is clearly visible in our β-N_2 spectra [marked by vertical dashed line in Fig. 1(b)]. By melting nitrogen crystal, it transfers to the hump observable in spectra of liquid nitrogen up to the boiling point. Earlier,[4,27] this feature in the β-N_2 phonon sideband spectra was assigned to a translational phonon mode (64 cm^{-1}).[28] However, the existence of a libron mode in the β-N_2 at high pressures, possessing close frequency values (50–60 cm^{-1}),[29] casts doubts on such an assignment. No fine structure exists in phonon sideband spectra of γ-O_2 as well as of liquid phases of both substances.

(ii) The phonon sideband spectra of α-oxygen and α-nitrogen [bottom of Figs. 1(a) and 1(b)] are characterized by almost the same intensity in spite of the fact that the nitrogen samples were 20 times thicker than the oxygen ones. This fact reflects the assistance in interaction between intramolecular and lattice excitations by a spin-spin exchange interaction in solid oxygen according to our opinion.[13]

(iii) The shape of the phonon sidebands is drastically changed at the orientationally order-disorder phase transitions in both substances—the β-γ phase transition in solid oxygen and the α-β one in solid nitrogen. The following increase in temperature causes no principal changes in the shape of the phonon sidebands. Very small quantitative changes are observed during melting.

(iv) Only the Stokes component is visible in the phonon sideband spectra at the lowest measured temperatures. An anti-Stokes part of the phonon sideband began to be detectable from 15 K in our spectra of solid nitrogen and from 18 K in the oxygen ones [shown by solid arrows in Figs. 1(a) and 1(b)]. As temperature increases, the intensity of this feature in the phonon sideband spectra increases too [e.g., see the spectrum at 35 K in Fig. 1(b)]. This feature is a mirror image of the Stokes part of the phonon sideband with respect to a frequency of the intramolecular vibrations. Due to the weakness of the anti-Stokes component of the phonon sideband spectrum, its shape reflects only the most intensive features of the Stokes one. In β-O_2, the anti-Stokes component manifests itself mainly as a low-frequency wing at the frequencies lower than the fundamental one. This wing was erroneously attributed in Ref. 24 to low-lying orientational

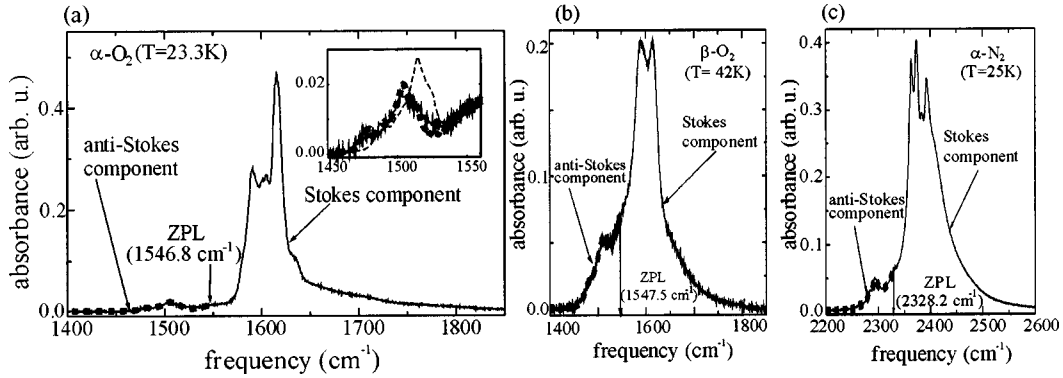

FIG. 2. Determination of the band origin frequency of the fundamental phonon sidebands (as ZPL) dividing the experimental sideband profiles into Stokes and anti-Stokes components: (a) and (b) solid oxygen, (c) α-nitrogen (for sake of clarity, the CO_2 peak is subtracted from the experimental profile—for details see text).

modes, which did not exist in this phase in principle. The spectrum at 42 K [Fig. 1(a)] demonstrates the feature in this frequency range (marked by a dashed arrow) that possesses the same origin as the one in the spectrum of the α-O_2 at 23 K. A similar situation takes place in β-nitrogen: the feature in the anti-Stokes part of the phonon sideband is clearly visible in the spectrum at 63 K [shown by a dashed arrow in Fig. 1(b)]. This shallow peculiarity of the phonon sideband profile reflects the maximum in the Stokes component of the phonon sideband lying at about 2390 cm^{-1}. In γ-O_2 and liquid phases of both substances, the anti-Stokes component of the phonon sideband reveals as a relatively steep low-frequency edge at frequencies lower than the fundamental one.

(v) Zero intensity is observed in the frequency range of the vibron excitations at the lowest measured temperatures. As temperature increases, the nonzero absorption appears at the vibron frequency (starting with 15 K in spectra of the solid nitrogen and with 23 K in the ones of solid oxygen) and continuously increases within the orientationally ordered phases (α-N_2, α- and β-O_2). This quality increases by a jump at the solid-solid phase transitions (α-β in N_2 as well as α-β and β-γ in O_2) and decreases further by increasing temperature within the orientationally disordered phases (β-N_2, γ-O_2, as well as liquids of both substances). Almost no discontinuity is observed in the absorption at the vibron frequency by melting nitrogen crystal, whereas a small positive jump in this quality is clearly detectable at this phase transition in oxygen. Although an excitation of a pure intramolecular vibration is not possible in ideal solid phases of both substances due to symmetry, the appearance of a nonzero absorbance at the vibron frequency is quite understandable at nonzero temperatures. Many-phonon processes allow the absorption of an incident light in orientationally ordered phases (e.g., the creation of one intramolecular vibration and one phonon plus the annihilation of one phonon with the same energy).[30] A substantially irregular orientational motion of molecules causes an interaction-induced absorption in the β-N_2 and γ-O_2 similarly to the one in liquids and compressed gases.[35(a)] In case of solid oxygen, dynamic fluctuations of magnetic order in the β-O_2 are presumably mainly responsible for the jump in the absorption at the vibron frequency observed at the α-β phase transition.

2. Modeling spectra and determination of the zero phonon line frequency

In general, an absorption spectrum of a phonon sideband to high-energetic transitions (electronic excitations, intramolecular vibrations) consists of two different parts—Stokes and anti-Stokes components—whose absorption intensities are related by the following simple equation:[13]

$$I_{\text{anti-Stokes}}(\omega_{\text{anti-Stoikes}}=\omega_0-\omega_{\text{ph}}) = I_{\text{Stokes}}(\omega_{\text{Stokes}}=\omega_0+\omega_{\text{ph}}) \times \exp(-\hbar\omega_{\text{ph}}/kT). \quad (1)$$

Here ω_0, ω_{ph} are the frequencies of an intramolecular excitation and a phonon involved, ω_{Stokes} and $\omega_{\text{anti-Stokes}}$ are the frequencies of the absorbed light due to additive (Stokes) and subtractive (anti-Stokes) combinations, and T is the sample temperature. If we presume that a phonon sideband is characterized by only *one* certain frequency ω_0 at each temperature (the so-called ZPL frequency), this value can be, in principle, determined from Eq. (1) by dividing an experimental profile of this absorption band into Stokes and anti-Stokes components. In this procedure, only *one* free parameter exists (a value of the ω_0 frequency) that must be obtained by comparing the modeled and experimental profiles of the anti-Stokes part of a phonon sideband. Consequently, a success in such modeling of experimental spectra may be considered as an experimental proof of the ZPL concept.

We tested this approach by modeling spectra of the phonon sidebands of intramolecular vibrational transitions in all phases of both oxygen and nitrogen. An excellent agreement between the experimental and modeled profiles was achieved by our procedure in all cases. The χ parameter characterizing an accuracy of a modeling procedure was as small as 10^{-6}–10^{-7} ($\chi=0$ corresponds to an ideal coincidence between measured and modeled spectra). Figure 2(a)–2(c) illustrate our results. Since a deviation between modeled and experimental profiles is too small to be recognized at such a scale of these figures, we marked the modeled profile of the anti-Stokes component by quadratic points.

The inset in Fig. 2(a) shows the anti-Stokes part of the phonon sideband at a substantially stronger magnification. It can be seen that this part of the band also possess the maxima, which mirror the most intensive features of the Stokes component but, of course, with opposite intensity ra-

tio due to the exponential factor in Eq. (1). The modeled profile (quadratic points) reproduces quite well these maxima in the anti-Stokes part of the experimental phonon sideband spectrum. The value of the ZPL frequency (1546.8 cm^{-1}) determined by our procedure deviates significantly from the vibron one (1552.6 cm^{-1}) measured by Raman scattering at this temperature. The dashed line in the inset in Fig. 2(a) shows the modeled profile of the anti-Stokes part of the phonon sideband spectrum if the Raman value is chosen as origin of the phonon sideband. No real agreement exists between the modeled and experimental profiles at such a choice. The comparison of these two cases [quadratic points and dashed line in the inset in Fig. 2(a)] validates a difference between the ZPL and vibron frequencies as well as illustrates the accuracy of our procedure to determine the ZPL frequency even at such a weak anti-Stokes component of the phonon sideband.

The statistical error of the ZPL frequency values obtained was less than 0.3 cm^{-1} in the α- and β-O_2 and less than 0.1 cm^{-1} in the γ-nitrogen and liquid oxygen. In the case of γ-O_2, we interpret the obtained ZPL frequency as the occupation-weighted mean of the two ZPL frequencies corresponding to disc-like (*d*) und spherelike (sp) molecules, i.e., $\omega_{\mathrm{ZPL}}^{\gamma\text{-}\mathrm{O}_2}=(3\omega_{\mathrm{ZPL}}^{d}+\omega_{\mathrm{ZPL}}^{\mathrm{sp}})/4$. In the orientationally disordered phases of both substances, the ZPL was always placed on the *low-frequency* edge of the experimental profile near to the main maximum of the phonon sideband spectra and approaches to its increasing temperature.

Our nitrogen gas contains a small amount of carbon dioxide as a residual contamination (~0.2 ppm). Due to very big oscillator strength of the ν_3-intramolecular transition of CO_2 molecules ($\omega_{\mathrm{gas}}^{\nu_3}=2349.16\ \mathrm{cm}^{-1}$),[32(b)] this absorption peak was clearly observable in our mid-ir spectra of solid and liquid nitrogen [marked by asterisk in Fig. 1(b)]. Besides these single-particle CO_2 excitations, a combination absorption band caused by simultaneously exciting the ν_3 vibrations of CO_2 molecules and lattice excitations of nitrogen matrix (nitrogen phonon sideband to ν_3 vibrations of CO_2 molecules) could affect our mid-ir spectra of nitrogen samples in principle. Consequently, we modeled the experimental profile of our mid-ir spectra of nitrogen samples [see, e.g., Fig. 3(a)] by three bands—two phonon sidebands (to internal vibrations of nitrogen and CO_2 molecules) and a single peak corresponding to the internal vibrations of CO_2 molecules [Fig. 3(b)]. To our knowledge, there is no direct information on the shape of the phonon sideband to the internal vibrations of CO_2 molecules matrix isolated in nitrogen. That is why we presumed that the shapes of the phonon sideband to internal vibrations of nitrogen and the one of CO_2 molecules are identical since both combination bands mainly map the phonon DOS function of the same substance (nitrogen).[33] The matrix isolated (MI) CO_2 peak was modeled by a Lorenz function (three adjustable parameters). Two other parameters, which had to be determined by our procedure, were a ZPL frequency of the nitrogen phonon sideband and a relation between the intensities of CO_2 and nitrogen phonon sidebands.

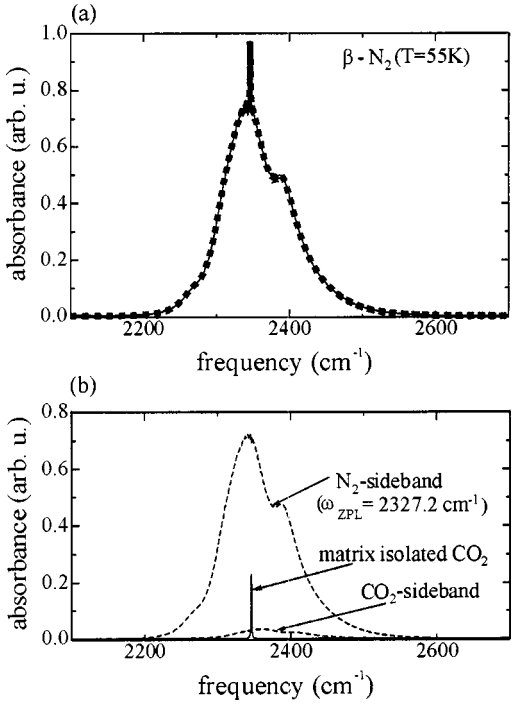

FIG. 3. Modeling the mid-ir experimental spectra of the β-nitrogen: (a) solid line—experimental spectrum, quadratic points—synthetic spectrum consisting of three bands shown in (b).

The agreement between the modeled (quadratic points) and experimental profiles (solid line) was excellent [Fig. 3(a)]. The statistical error of the ZPL frequency values obtained was less than 0.07 cm^{-1} in the α-N_2 and less than 0.04 cm^{-1} in other phases. Importantly, the ZPL frequency values of the β-nitrogen and liquid nitrogen increase if the CO_2 phonon sideband is deliberately not included by modeling the experimental spectra. Utilizing our values of the ZPL frequencies in β-N_2, we could also classify the kind of lattice excitations, which are responsible for the feature in the fundamental phonon sideband spectra of this nitrogen phase [marked by dashed line in Fig. 1(b)]. The frequency of these excitations, determined as the difference between the frequency of the maximum of this feature and the ZPL one, decreases from 64 cm^{-1} at 36 K to 57.5 cm^{-1} at 63 K. Taking in account the known thermal expansion of β-N_2,[34] we obtain the corresponding Grüneisen constant value of 1.88 ± 0.04, which is the characteristic quantity for libron excitations.[16] Consequently, we associate this singularity in the phonon sideband spectra of β-N_2 with nutational motion of N_2 molecules (orientational oscillations of molecular axes relative to the *c* axis of hcp structure). That is, a libronlike mode actually exists in this nitrogen phase at ambient pressure that was supposed early,[34] based on the thermodynamic analysis.

The absolute absorption coefficient of the intramolecular transition in CO_2 molecules determined by our procedure was $0.04\pm0.006\ \mathrm{cm}^{-2}$, and did not show any definite temperature dependence. Using our previous results,[6,31] we estimated the concentration of CO_2 molecules in our samples of solid and liquid nitrogen as to be of about 0.2 ppm. The phonon sideband to the internal vibrations of CO_2 molecules

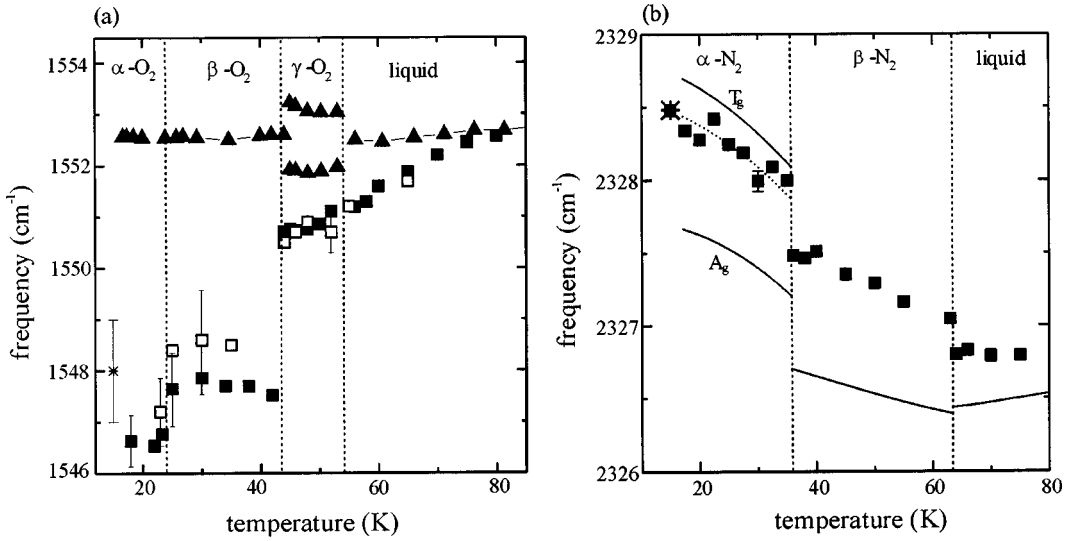

FIG. 4. Temperature dependence of the frequencies of internal vibrations of oxygen (a) and nitrogen (b). Filled quadrates mark the ZPL frequency of the fundamental phonon sideband, up triangles and solid lines—Raman vibron mode frequencies of oxygen (present work) and nitrogen (Ref. 25), respectively [inaccuracy $<0.02\ \mathrm{cm}^{-1}$], dotted line in (b)—the degeneracy-weighted mean of the frequency of two Raman vibron modes of α-N_2, asterisks—the fundamental frequencies of *single* molecules in isotope-mixed crystals, empty quadrates—the fundamental frequency of *single* molecules deduced by analyzing the phonon sideband to the first vibrational overtone (for details see text).

possesses practically zero intensity in the orientationally ordered α-N_2. After the α-β phase transition, this quantity becomes non-negligible and increases due to temperature. The ratio of the intensities of the CO_2 and nitrogen phonon sidebands is changed from 0.0035 ± 0.001 at 36 K to 0.11 ± 0.008 at 75 K, whereas the intensity of nitrogen phonon sideband slightly decreases (of about 10%) in this temperature range. Such a behavior of an impurity phonon sideband would be quite understandable in orientationally ordered phases, where such an effect reflects the increasing occupation of excited librational states due to temperature. Recently,[31] we discovered that axes of matrix isolated CO_2 molecules are firmly oriented relative to the *c* axis of the β-N_2. Our present results additionally indicate the existence of a local orientational order of nitrogen molecules around CO_2 impurities in both disordered nitrogen phases (β and liquid).

A success in modeling the ir-active phonon sideband spectra to internal vibrations in all investigated phases of both substances (Figs. 2 and 3) shows that the ZPL concept reflects the real situation in molecular crystals and allows us to describe an experimental profile correctly.

3. Comparison between ir and Raman data

Figure 4 shows the ZPL frequency values determined by our procedure (filled quadrates) as well as the available Raman data on the vibron frequencies (up triangles—present work, solid lines—Ref. 25) and on the fundamental frequencies of *single* molecules isolated in the isotope-mixed α-oxygen[36] and α-nitrogen[37] (asterisks). The following general features can be seen by analyzing Fig. 4.

(i) The values of the ZPL frequency (ω_{ZPL}) by FTIR disagree significantly with the vibron frequencies (ω_{vib}) at the center of the Brillouin zone by Raman and are in accord with the isotope ones in both substances. The greatest difference between the vibron and ZPL frequencies ($\Delta\omega=\omega_{\mathrm{vib}}-\omega_{\mathrm{ZPL}}$) is observed in the α- and β-O_2 (about $+5\ \mathrm{cm}^{-1}$), while these quantities almost coincide in liquid oxygen, near the boiling point [Fig. 4(a)]. The $\Delta\omega$ values are positive in all phases of oxygen and negative in the β and liquid nitrogen.

(ii) The ZPL frequency possesses no observable temperature dependence in the α- and β-O_2 similarly to the vibron one. This quality strongly raises increasing temperature in the γ-and liquid oxygen while very small temperature-caused changes are observed in the vibron frequencies in these oxygen phases [Fig. 4(a)]. The temperature behavior of the ZPL frequency is qualitatively similar to the one of vibron frequencies in both phases of solid nitrogen. However, the difference between these two quantities possesses a clear temperature dependence, especially in β-N_2 [Fig. 4(b)]

(iii) The ZPL frequency is changed by jump at each solid-solid phase transition of both substances as well as at the melting of the nitrogen crystal. The most drastic changes in this quality occur at the β-γ phase transition in oxygen [$\Delta\omega_{\mathrm{ZPL}}(T_{\gamma\text{-}\beta})\approx3\ \mathrm{cm}^{-1}$] to compare to the quite moderate jump in the vibron frequencies [$\Delta\omega_{\mathrm{vib}}(T_{\gamma\text{-}\beta})\sim0.5\ \mathrm{cm}^{-1}$] according to our precise Raman measurements.

This qualitative comparison between the vibron and ZPL frequencies shows clearly that it actually deals with two different physical qualities. Although both qualities characterize the internal vibrations of the molecules in condensed media, they possess different concrete values and sense variously the changes in the crystal when external parameters (temperature in our case) are varied. Let us discuss now the physical meaning of the band origin frequency (as ZPL) of an ir-active phonon sideband. During this discussion, we must keep in mind that this question is intimately related to the more general problem of the nature of such a combina-

tion band. We think of two possible physical pictures.

First. An ir-active phonon sideband is formed by the interaction between two kinds of quasiparticles—vibrons and phonons. To fit this interpretation to the ZPL concept we have to suppose that most part of the vibron density of states is concentrated in a very narrow frequency range close to the ZPL frequency value, which we determined by analyzing the experimental phonon sideband profile. We cannot rule out the existence of such a special form of the vibron DOS *a priori*. However, the vibron DOS function of the α-nitrogen[39] possesses no such strong singularity.

Second. An interaction between internal vibrations of *single* molecules and lattice excitations is responsible for the appearance of an ir-active phonon sideband. That is, the phonon sideband in pure crystals possesses the same physical origin as the one to intramolecular excitations of impurity centers in doped crystals.[40] The good agreement between the values of ZPL frequency and fundamental one of isolated isotope molecules counts in favor of this physical picture. A similar physical approach was suggested in Ref. 7 to explain the phonon sideband structure in electronic absorption spectra of molecular crystals.

In principle, the second scenario could be simply proven by comparing the ZPL frequency, obtained by our procedure, to the frequency of internal vibrations of *single* molecules in the investigated substances, if the latter frequency would be known from some independent measurements. To our knowledge, such information is available for α-N_2 only. According to a theoretical analysis,[41] the degeneracy-weighted mean of the frequencies of two (T_g and A_g) vibron modes is practically equal to the frequency of internal vibrations of single nitrogen molecules in this phase [shown by a dotted line in Fig. 4(b)]. A quite good agreement between these literature data and our values of the ZPL frequency (quadrates) strongly supports the second mechanism. To find convincing proofs, supporting this physical picture, we carried out a general theoretical analysis of the vibron energy zones as a function of the vibrational quantum number and discovered the possibility to determine the frequency of internal vibrations of *single* molecules ($\omega^s_{0\text{-}n}$) in crystal from the experimental spectra directly.

B. Vibron excitations: theoretical background

Treating intramolecular vibrations in a molecular solid as low-energetic Frenkel excitons,[8] we can express the frequency of these excitations in a crystal in the following form:

$$\omega^{\rm cr}_{0\text{-}n}(\mathbf{k}) = \omega^{\rm gas}_{0\text{-}n} + D_{0\text{-}n} + M_{0\text{-}n}(\mathbf{k}). \tag{2}$$

Here n is the vibrational quantum number, $\omega^{\rm cr}_{0\text{-}n}(\mathbf{k})$ and $\omega^{\rm gas}_{0\text{-}n}$ are the frequencies of the $0\text{-}n$ internal vibrational transition in the crystal and in the free molecule, respectively ($\mathbf{k}$ is a wave vector of these excitations in a crystal), $D_{0\text{-}n}$ describes the change in the energy of this transition in a *single* molecule because of its interaction with surrounding particles in a condensed medium (the so-called ''environmental'' frequency shift), $M_{0\text{-}n}(\mathbf{k})$ is the term arising due to an exchange of excitations between *identical* molecules. This term is responsible for the width of the vibron energy zone and usually called ''resonance'' frequency shift.

Both the environmental and resonance shifts are caused by the intermolecular interaction. Expanding the potential energy of the crystal into a Taylor series of internal normal vibrational coordinates and restricting it to quadratic terms we obtain the following formulas for the environmental and resonance frequency shifts that generalize the well-known expressions[42] here now for arbitrary intramolecular potential,

$$D_{0\text{-}n} = [\langle n|u|n\rangle - \langle 0|u|0\rangle]\left(\frac{\partial U_{\rm cr}}{\partial u_i}\right)_{u_i=0} + \frac{1}{2}[\langle n|u^2|n\rangle - \langle 0|u^2|0\rangle]\left(\frac{\partial^2 U_{\rm cr}}{\partial u_i^2}\right)_{u_i=0}, \tag{3a}$$

$$M_{0\text{-}n}(k=0) = \langle n|u|0\rangle^2 \sum_j \left(\frac{\partial^2 U_{\rm cr}}{\partial u_i \partial u_j}\right)_{u_i=0,u_j=0}. \tag{3b}$$

$U_{\rm cr}$ is the potential energy of the crystal averaged over translational and orientational motions of the molecules; u_i is the normalized internal vibrational coordinate of the ith molecule [$u=(r-r_e)/r_e$]; r and r_e are the instantaneous and equilibrium bond lengths, respectively; $|n\rangle$ and $|0\rangle$ are the wave functions of the nth and ground (0) internal vibrational molecular states.

It is known[43] that the Morse potential [$V(u)=E_e(e^{-2\alpha u}-2e^{-\alpha u})$] describes excellently internal vibrations of diatomic molecules in both ground and low-lying excited vibrational states. Then, using the analytical expressions for the eigenfunctions of a Morse oscillator,[44] we can express the matrix elements given in Eq. (3) in an analytic form suitable for practical calculations. Equating the eigenvalues of a Morse oscillator to the first two terms of the experimental vibrational spectrum (the contribution of higher terms is usually small[45]), we related the Morse dissociation energy E_e and the Morse parameter α to the well-known spectroscopic characteristic of diatomic molecules: $E_e=\omega_e^2/(4\omega_e x_e)$, $\alpha=(\omega_e x_e/B_e)^{1/2}/r_e$ [$\omega_e x_e$ is the anharmonic vibrational constant]. Further, considering x_e as a small parameter ($x_e<10^{-2}$ for molecules of interest), we expanded the expressions for the matrix elements of interest into a Taylor series and kept the leading terms only. The final formulas obtained are presented in Table I for $n\leqslant 3$.

Putting these formulas into Eqs. (3) and comparing expressions obtained at different vibrational quantum numbers, we can deduce important relations linking the environmental and resonance shifts of high-excited vibrational states to the corresponding values for fundamental vibrations,

$$D_{0\text{-}n} \cong n D_{0\text{-}1}, \quad M_{0\text{-}n}(k=0) = a_n (x_e)^{n-1} M_{0\text{-}1}(k=0), \tag{4}$$

where a_n is a numerical coefficient of the order of 1.

Since x_e is very small, the resonance term $M_{0\text{-}n}$ vanishes at $n\geqslant 2$. That is, the vibron energy zones of high-excited vibrational states may be considered as dispersionless for any practical purposes,

TABLE I. Matrix elements acting in the environmental and resonance frequency shifts of intramolecular vibrations [see Eqs. (3)] for different vibrational quantum numbers (Morse potential).

n	$\langle n\|u\|n\rangle-\langle 0\|u\|0\rangle$	$\langle n\|u^2\|n\rangle-\langle 0\|u^2\|0\rangle$	$\langle n\|u\|0\rangle^2$
1	$3\left(\frac{B_e x_e}{\omega_e}\right)^{1/2}(1+2x_e+\cdots)$	$2\frac{B_e}{\omega_e}(1+6x_e+\cdots)$	$\frac{B_e}{\omega_e}(1+x_e+\cdots)$
2	$6\left(\frac{B_e x_e}{\omega_e}\right)^{1/2}\left(1+\frac{7}{2}x_e+\cdots\right)$	$4\frac{B_e}{\omega_e}\left(1+\frac{21}{2}x_e+\cdots\right)$	$\frac{B_e x_e}{2\omega_e}(1+3x_e+\cdots)$
3	$9\left(\frac{B_e x_e}{\omega_e}\right)^{1/2}\left(1+\frac{14}{3}x_e+\cdots\right)$	$6\frac{B_e}{\omega_e}(1+14x_e+\cdots)$	$\frac{2}{3}\frac{B_e}{\omega_e}x_e^2[1+\mathrm{O}(x_e)]$

$$\omega_{0\text{-}n}^{\mathrm{cr}} \cong \omega_{0\text{-}n}^{\mathrm{gas}} + D_{0\text{-}n} \equiv \omega_{0\text{-}n}^{s} \quad (n \geqslant 2). \tag{5}$$

Then, using Eqs. (4), (5), the frequency of fundamental vibrations of *single* molecules in a crystal can be simply reconstructed from the one of the vibrational overtone if the last value is known, e.g., $\omega_{0\text{-}1}^{s} = \omega_{0\text{-}1}^{\mathrm{gas}} + (\omega_{0\text{-}2}^{\mathrm{cr}} - \omega_{0\text{-}2}^{\mathrm{gas}})/2$. Since we could not find any literature data of the frequency values of vibrational overtones in condensed phases of our substances, we carefully measured the ir-active phonon sidebands to the first vibrational overtone to determine the $\omega_{0\text{-}2}^{\mathrm{cr}}$ frequencies as the ZPL of these phonon sidebands by applying our procedure.

C. Phonon sidebands to the first vibrational overtone

Figure 5 shows the temperature evolution of the absorption spectra in the spectral region of the first vibrational overtone in oxygen (a) and nitrogen (b). The dashed vertical lines mark the frequencies of the vibrational overtone in free molecules for comparison. The nitrogen spectra in this spectral region were already measured by other investigators,[46] while the oxygen ones were investigated by us.

Comparing the spectra in overtone spectral region (Fig. 5) to the ones in the fundamental region (Fig. 1), four general features are clearly visible.

(i) The phonon sideband spectra to the first vibrational overtone are by about two orders of magnitude less intensive than the one to the fundamental vibration. This numerical value possesses the same order of magnitude as the usual ratio of intensities of fundamental and overtone vibrations in case of ir-active linear molecules [e.g., $(I_{0\text{-}1}/I_{0\text{-}2})_{\mathrm{CO}} = 130$].[47]

(ii) Both kinds of sidebands possess very similar band profiles. This similarity is most pronounced in α-O_2, whose spectra are characterized by almost identical fine structure in the fundamental and overtone frequency regions [bottom spectra in Figs. 1(a) and 5(a)]. The anti-Stokes part is clearly visible in the overtone phonon sideband spectra of α-O_2 at 23 K [an arrow in Fig. 5(a)] similarly to the one in the fundamental spectral region [Fig. 1(a)].

(iii) An additional broad feature appears in the spectra of the orientationally disordered phases of both substances in the overtone spectral region [marked by asterisks in Fig. 5(a)] besides the phonon sideband to vibrational overtone.

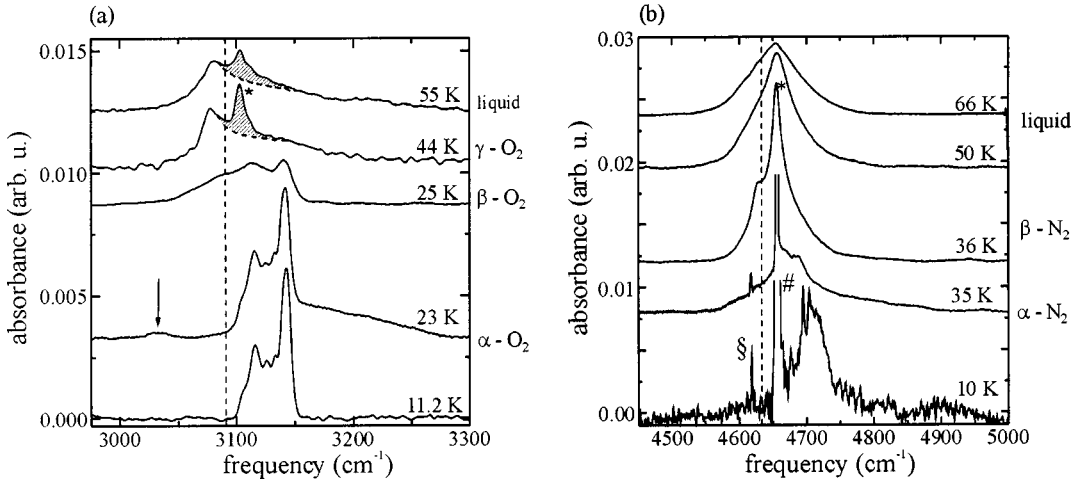

FIG. 5. Temperature evolution of the absorption spectra of oxygen (a) and nitrogen (b) in spectral region of the first vibrational overtone. Vertical dashed lines mark the frequency of the first vibrational overtone of free molecules. The absorption bands due to a simultaneous excitation of internal vibrations of two molecules are marked by asterisks [(a), (b)] as well as are shown by shaded areas in (a). Labels # and § (b) mark the two-vibron band as well as the band due to simultaneous excitation of the vibron mode of $^{14}N_2$ and internal vibrations of $^{14}N^{15}N$ isotope, respectively.

TABLE II. Frequencies of peculiarities of the phonon sidebands to the fundamental molecular vibrations and to the first overtone in the *a*-oxygen, $T=23$ K (inaccuracy is less than 0.5 cm^{-1}).

Frequency of peculiarities (cm^{-1})				
Fundamental phonon sideband		First overtone phonon sideband		
Absolute value	With respect to the band origin ($\omega_{ZPL}^{0\text{-}1}=1546.8$ cm^{-1})	Absolute value	With respect to the band origin ($\omega_{ZPL}^{0\text{-}2}=3069.8$ cm^{-1})	Assignment[a]
1590.9	44.1	3115.2	45.4	Libron
1601	54.2	3124.8	55	Phonon
1606.1	59.3	3131.1	61.3	Phonon
1616.9	71.1	3141.7	71.9	Libron+phonon

[a]Reference 13.

This additional band possesses an asymmetric profile qualitatively similar to the one of the phonon sideband. The maximum of this feature is at 3102 cm^{-1} in spectra of γ-O_2 ($T=44$ K) and at about 4655 cm^{-1} in β-N_2 spectra. These values are practically twice of the ZPL frequency of the fundamental vibrations (see Fig. 4). Consequently, we assigned these additional bands to a simultaneous vibrational absorption by two neighboring molecules induced by intermolecular interaction. Similar in-active bands were earlier observed in compressed gas mixtures.[35(b)] That is, two different kinds of combined processes act in the vibrational overtone region in absorption: a combined excitation of an intramolecular vibrational overtone and lattice vibrations (the phonon sideband to the vibrational overtone) as well as a simultaneous excitation of internal vibrations of two molecules (simultaneous vibrational absorption).[48] The intensity of second band strongly decreases with increasing temperature, whereas the one of the phonon sideband to vibrational overtone shows a substantially weaker temperature dependence [see, e.g., spectra of γ-oxygen and liquid oxygen in Fig. 5(a), where both bands are well separated]. Both physical mechanisms cause a comparable contribution to the total absorption of nitrogen in this spectral region [Fig. 5(b), β-nitrogen and liquid nitrogen], whereas the overtone phonon sideband dominates in oxygen spectra, especially at higher temperatures [Fig. 5(a), $T=55$ K]. Moreover, the band due to a simultaneous vibrational absorption is about three times broader in nitrogen phases (width ≈ 70 cm^{-1}) than in oxygen phases (width $\leqslant 25$ cm^{-1}).

(iv) Two additional bands are clearly visible in the overtone spectra of α-nitrogen next to the overtone phonon sideband [bottom spectra in Fig. 5(b)]. These bands are centered at 4618.5 and 4657 cm^{-1} (10 K) and are formed by similar processes. The extremely strong second band (marked by #) arises by a simultaneous excitation of two vibron modes of α-$^{14}N_2$ crystal (T_g+A_g) by one photon,[46,49] while the first band (marked by §) corresponds to a simultaneous excitation of fundamental vibrations of $^{15}N^{14}N$ isotopes and a vibron mode of $^{14}N_2$ crystal.[49]

The existence of intensive additional bands, whose exact shapes are unknown, did not allow us to apply our procedure (Stokes/anti-Stokes deconvolution to find ZPL, Sec. III A) to analyze spectra of nitrogen phases in this region quantitatively. However, we had no problems analyzing the overtone spectra of α-and β-oxygen. Moreover, the additional feature can be relatively simply subtracted from the experimental overtone spectra of γ-nitrogen and liquid oxygen, since it is not too broad and, consequently, easily distinguishable from the phonon sideband spectrum. At our subtracting procedure, we supposed that the shape of the phonon sideband to the vibrational overtone is identical to the one to the fundamental vibration as it is practically the case in the low-temperature phases of solid oxygen. In addition, we divided these overtone phonon sideband spectra into Stokes and anti-Stokes components and determined the frequency $\omega_{0\text{-}2}^{cr}$ of the overtone internal vibrations (as ZPL).

Using the obtained $\omega_{0\text{-}2}^{cr}$ quantities, we calculated (see preceding paragraph) the values of the fundamental frequency of single molecule excitations ($\omega_{0\text{-}1}^{s}$) in solid and liquid oxygen and compared those to the frequency of the ZPL of the fundamental phonon sideband [empty and filled quadrates in Fig. 4(a)]. A very good agreement exists between these two sets of data in *all* condensed phases of oxygen. Table II shows that the same lattice modes are responsible for singularities in the phonon sideband spectra, both in the fundamental and in the overtone spectral regions, as expected. These results represent the *conclusive* proof that the ZPL of an ir-active fundamental phonon sideband corresponds to the fundamental frequency of *single* molecules in condensed media.

In general,[8] both terms acting in the frequency of the internal vibrations in pure crystal [D and M in Eq. (2)] can contribute to a vibron-phonon coupling (mechanical or optical anharmonicity) through their dependence upon the intermolecular coordinates changed by both angular and translational motion of molecules [see Eqs. (3)]. Our experimental results mean that the interaction between the intra-molecular and intermolecular vibrations arises in a crystal *explicitly* (or at least mainly) because of the variations of the environmental frequency shift [D term in Eq. (2)] by molecular motion, whereas the variations of the resonance frequency shift [M term in Eq. (2)] cause a negligible contribution to this coupling.

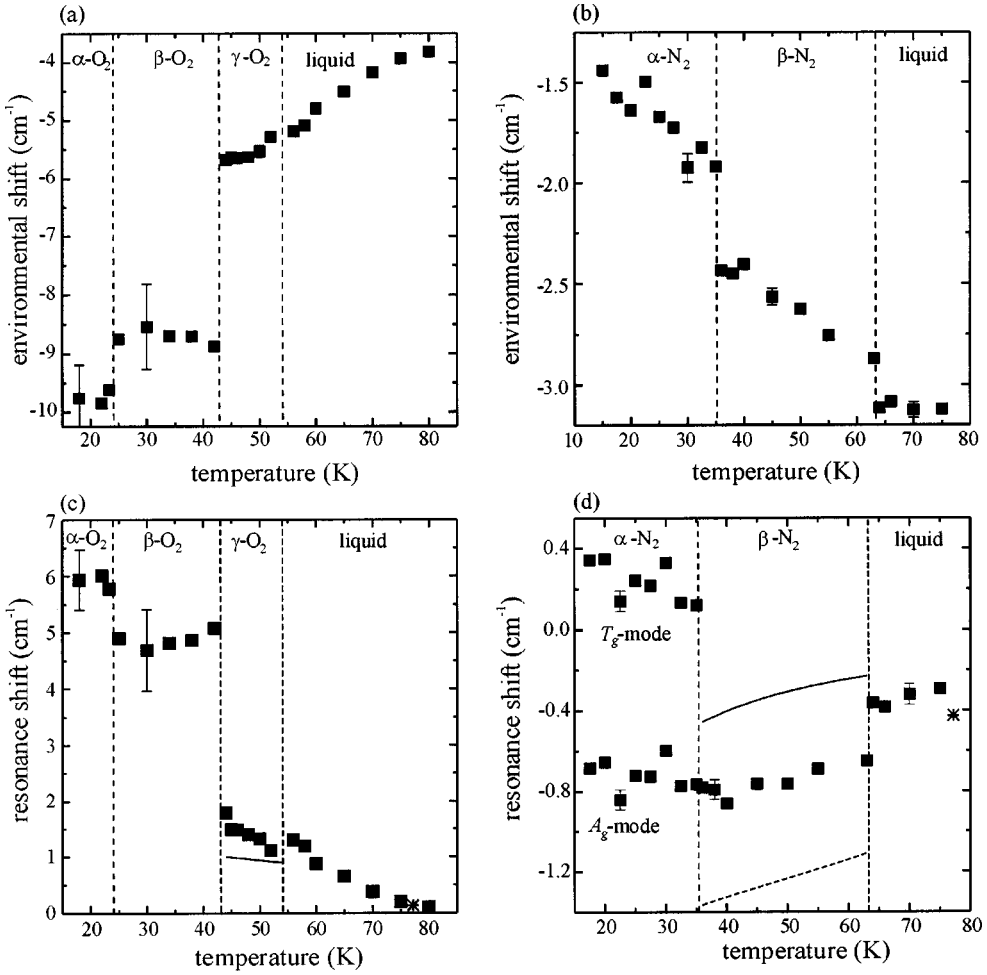

FIG. 6. Characteristics of the fundamental vibron energy zones: environmental frequency shift ($D_{0\text{-}1}$) in oxygen (a) and nitrogen (b), resonance frequency shift [$M_{0\text{-}1}(\mathbf{k}=0)$] in oxygen (c) and nitrogen (d). In the case of γ-O_2, the occupancy-weighted mean of the corresponding quantities for two vibron modes existed (spherelike and disklike molecules) are shown. Symbols indicate experimental data: filled quadrates—present work, asterisks—Ref. 49. Lines [(c), (d)] show our theoretical results—solid and dashed lines in (d) indicate the lower [Eq. (15)] and uppermost [Eq. (13)] estimates of the resonance frequency shift in β-N_2.

D. Fundamental vibron energy zone

A complete set of experimental data—the vibron frequencies $\omega^{\text{vib}}_{0\text{-}1}(\mathbf{k}=0)$ (Raman) and the ZPL frequency $\omega^{s}_{0\text{-}1}$ (infrared)—allows us to characterize the fundamental vibron energy zone in crystal quantitatively without any theoretical modeling. Indeed, the environmental and resonance frequency shifts can be directly reconstructed [see Eq. (2)] from experimental data,

$$D_{0\text{-}1}=\omega^{s}_{0\text{-}1}-\omega^{\text{gas}}_{0\text{-}1}, \tag{6a}$$

$$M_{0\text{-}1}(\mathbf{k}=0)=\omega^{\text{vib}}_{0\text{-}1}(\mathbf{k}=0)-\omega^{s}_{0\text{-}1}. \tag{6b}$$

The environmental frequency shift locates a vibron energy zone in crystal with reference to the gas value of internal vibrations, while the resonance frequency shift at $\mathbf{k}=0$ gives a quite good estimate of the whole width W_{vib} of this zone (if a Davydov splitting is absent). For example, $W_{\text{vib}}=(4/3)|M_{0\text{-}1}|$ for fcc and hcp structures.[42(b)]

Introducing the ZPL and vibron frequency values (Fig. 4) as well as the gas values of the fundamental frequency[32(b)] into Eq. (6), we determined the environmental and resonance frequency shifts in all phases of both substances at ambient pressure (quadrates in Fig. 6). Before our measurements, such experimental information was only available for the resonance frequency shift in liquid oxygen and nitrogen[50] ($T=77.35$ K) [asterisks in Figs. 6(c) and 6(d)]. These data fit our results quite well. We trace a small discrepancy in the resonance shift values of liquid N_2 [Fig. 6(d)] back to some uncertainty of our procedure subtracting the CO_2 sideband from experimental spectra (see Sec. III A 2).

Both characteristics [$D_{0\text{-}1}$ and $M_{0\text{-}1}(\mathbf{k}=0)$] of vibron energy zone demonstrate very strong but opposite temperature behavior in oxygen [Figs. 6(a) and 6(c)]. As a results, the vibron frequencies that are actually composed of the environmental and resonance frequency shifts (plus gas value) possess almost no temperature dependence from 5 K to the boiling point [see Fig. 4(a), triangles]. In case of nitrogen, the environmental frequency shift [Fig. 6(b)] changes substantially stronger due to temperature than the resonance one [Fig. 6(d)]. That is, the measured temperature behavior of its vibron frequencies [see Fig. 4(b), solid lines] is mostly

caused by changes in the environmental frequency shift. Let us analyze the environmental and resonance frequency shift behavior in more detail.

1. Environmental frequency shift

Although the environmental shift of the fundamental frequencies possesses negative values in both substances, the general temperature behavior is quantitatively different in condensed phases of oxygen and nitrogen [Figs. 6(a) and 6(b)]. In case of nitrogen, this quality continuously decreases with increasing temperature in α- and β-N_2 and flattens out in liquid nitrogen. Since the vibron frequency goes up in liquid N_2 (Ref. 25) and since the resonance frequency shift becomes relatively small already at 77 K [see Fig. 6(d)], we are expecting a rise in the environmental shift values of liquid nitrogen approaching the critical point. Consequently, the case of zero-pressure nitrogen phases corresponds to a typical situation when an environmental frequency shift possesses an *U*-like dependence on density.[51] In case of oxygen [Fig. 6(a)] the environmental frequency shift shows a general trend to increase due to temperature (decreasing density). Such a behavior reproduces qualitatively a low-density part of the corresponding dependence in other substances. It means that a minimum of the environmental frequency shift is either already reached in the α-O_2 at ambient pressure or is located somewhere in the high-pressure region. Let us give a qualitative explanation of the observed behavior of the environmental frequency shift in both substances.

The environmental frequency shift was previously theoretically analyzed[41] in α- and γ-N_2 as a function of molar volume at zero temperature. It was shown that this quality is mostly governed by a competition between the contributions due to the dispersion and repulsion parts of the intermolecular interaction in solid nitrogen, which possess opposite signs: $D_{0\text{-}1}^{\mathrm{disp}}$ is negative, whereas $D_{0\text{-}1}^{\mathrm{rep}}$ is positive.[52] Since the repulsive interaction possesses a substantially stronger dependence on the intermolecular separation R (e.g., $\sim R^{-12}$) than the dispersion one ($\sim R^{-6}$), the decrease in the experimental $D_{0\text{-}1}$ values [Fig. 6(b)] is caused by a relative weakening of the repulsion interaction due to thermal expansion of the nitrogen crystal. In the liquid nitrogen, a contribution of the repulsive interaction becomes very small and the environmental shift is almost completely determined by the dispersion part of the intermolecular interaction ($D_{0\text{-}1}^{\mathrm{disp}}$ term) whose absolute value slowly decreases with decreasing density (increasing temperature).

To our knowledge, there are no theoretical works concerning vibron excitations of solid oxygen at zero pressure. Therefore, we will base our following discussion upon the fact that the structure of the derivatives of the potential energy used in Eq. (3a) is usually qualitatively similar to the one of the potential energy itself. Since the crystal structures of α- and β-O_2 are explicitly stabilized by the *anisotropic* part of the repulsive interaction,[20] we may conclude that this term in potential energy is responsible for the large negative environmental frequency shift in these oxygen phases. This interaction decreases by a big jump at the β-γ transition because of the drastic molar volume changes as well as the radical reconstruction of the crystal structure. As a result, the environmental frequency shift also increases by a big jump. The following temperature-caused changes can be mainly explained by a weakening of the dispersion part of the intermolecular interaction due to thermal expansion similarly to the case of liquid nitrogen.

2. Resonance frequency shift

This quality is positive in all oxygen phases [Fig. 6(c)] and negative in the β-nitrogen and liquid nitrogen [Fig. 6(d)]. That is, vibron excitations are characterized by a positive effective mass in these nitrogen phases and a negative one in all phases of oxygen. Since a resonance frequency shift characterizes a strength of the collective effects in condensed media, of particular interest is to understand its origin in both substances. In general, the resonance frequency shift consists of two components ($M_{0\text{-}1}^{\mathrm{is}}$ and $M_{0\text{-}1}^{\mathrm{anis}}$) related to the isotropic and anisotropic parts of potential energy of crystal, respectively,

$$M_{0\text{-}1}(\mathbf{k}=0) \equiv M_{0\text{-}1}^{\mathrm{is}}(\mathbf{k}=0) + M_{0\text{-}1}^{\mathrm{anis}}(\mathbf{k}=0). \tag{7}$$

The $M_{0\text{-}1}^{\mathrm{is}}$ term corresponds to the situation if the molecules are completely orientationally disordered while the second one is explicitly caused by the correlations in the molecular orientational motion. Its ($M_{0\text{-}1}^{\mathrm{anis}}$) numerical value depends on the character and strength of the long- or short-range orientational order. Let us start our discussion with nitrogen.

The $M_{0\text{-}1}^{\mathrm{is}}$ value in the α-N_2 can be directly estimated from available experimental data. Introducing Eq. (7) into Eq. (2) and using the general formalism of Ref. 41, the Raman mode frequencies in α-N_2 can be written as follows ($M_{\mathrm{equiv}}^{\mathrm{anis}}$ and $M_{\mathrm{diff}}^{\mathrm{anis}}$ are the anisotropic parts of the resonance interaction between the molecules within one sublattice and from different sublattice, respectively, $\omega_{0\text{-}1}^{s}$ is the fundamental frequency of *single* molecules):

$$\omega_{A_g} = \omega_{0\text{-}1}^{s} + M_{0\text{-}1}^{\mathrm{is}}(\mathbf{k}=0) + M_{\mathrm{equiv}}^{\mathrm{anis}}(\mathbf{k}=0) + M_{\mathrm{diff}}^{\mathrm{anis}}, \tag{8a}$$

$$\omega_{T_g} = \omega_{0\text{-}1}^{s} + M_{0\text{-}1}^{\mathrm{is}}(\mathbf{k}=0) + M_{\mathrm{equiv}}^{\mathrm{anis}}(\mathbf{k}=0) - M_{\mathrm{diff}}^{\mathrm{anis}}/3. \tag{8b}$$

The term of $M_{\mathrm{equiv}}^{\mathrm{anis}}$ is small ($|M_{\mathrm{equiv}}^{\mathrm{anis}}| < 0.1\ \mathrm{cm}^{-1}$)[41] and can be omitted. Then

$$M_{0\text{-}1}^{\mathrm{is}}(\mathbf{k}=0) \simeq (\omega_{A_g} + 3\omega_{T_g})/4 - \omega_{0\text{-}1}^{s}. \tag{9}$$

Introducing the ω_{A_g} and ω_{T_g} values[38] as well as the $\omega_{0\text{-}1}^{s}$ value[37] into Eq. (9), we obtain the value $M_{0\text{-}1}^{\mathrm{is}}(\mathbf{k}=0) \approx -0.12\ \mathrm{cm}^{-1}$ as an estimate of the isotropic component of the resonance frequency shift in α-N_2. Because the c/a parameter in the β-N_2 deviates very weakly from the one of an ideal hcp structure,[34] this quality possesses practically the same numerical values in both closed-packed (α, β) phases of nitrogen. Comparing this value to the experimental ones [$\approx -0.8\ \mathrm{cm}^{-1}$ in β-N_2 and $\approx -0.4\ \mathrm{cm}^{-1}$ in liquid N_2, see Fig. 6(d)], we conclude that orientational correlations mainly cause the observed resonance frequency shift in both β-nitrogen and liquid nitrogen. In case of α-N_2, a measure of an anisotropic part of the resonance frequency shift is the T_g-A_g frequency splitting explicitly caused by the existence

of long-range orientational order in this nitrogen phase. This splitting decreases from 1.05 cm^{-1} at 6 K to 0.89 cm^{-1} at 35 K.[53] The last value is very close to the absolute value of the resonance shift in β-N_2 near the α-β phase transition point [Fig. 6(d)]. It means that the strength of orientational correlations (orientational order parameter) is almost identical in both solid phases of nitrogen at the α-β phase transition. Very weak changes in the resonance frequency shift values (from -0.8 cm^{-1} at 36 K to -0.7 cm^{-1} at 63 K) indicate that the short-range orientational order is only little affected due to temperature within the whole temperature range of β-N_2. A considerable resonance frequency shift in liquid N_2 points to a persistence of strong orientational correlations between nearest neighbors in liquid nitrogen up to the normal boiling point.

The absolute values of the resonance frequency shift $[M_{0\text{-}1}(\mathbf{k}=0)]$ are very large (~ 5 cm^{-1}) and possess almost no temperature dependence in the orientationally ordered α and β phases of oxygen [see Fig. 6(c)]. Considering the nature of stability of these oxygen phases[15,20] (see also preceding paragraph), we trace these large positive values of $M_{0\text{-}1}(\mathbf{k}=0)$ in α-and β-O_2 back to the dominant role of the anisotropic term in Eq. (8). At the β-γ phase transition, the resonance frequency shift undergoes a big jump ($\geqslant 3$ cm^{-1}) and strongly decreases with increasing temperature up to 0.1 cm^{-1} in liquid oxygen at 80 K. Due to the existence of two kinds of molecules in γ-O_2 (spherelike and disclike molecules), the origin of this quality is not obvious in this oxygen phase. To clarify it, we carried out the theoretical analysis of the resonance frequency shift in γ-O_2 using Eq. (3b) and the corresponding matrix element from Table I. At the concrete calculations, performed by a symbolic algebra program (MAPLE V, Release 5), we based on the model of ''discs and spheres'' [20] and used the intermolecular potential[26(b)] as well as the lattice parameter.[19] Since we could not find any information on the derivative of the quadrupole moment Q of the oxygen molecule with respect to its bond length, we presumed that the quantity $\partial \ln Q/\partial \ln r$ is the same in case of nitrogen and oxygen molecules: $(\partial \ln Q/\partial \ln r)_{O_2} \approx (\partial \ln Q/\partial \ln r)_{N_2} = -1.93$.[54] An arbitrariness of such a choice does not affect significantly our results because of a very small contribution of this electrostatic component to the qualities of interest (see Table III). The lattice sums were taken up to $R_{ij}=2R_0$ (R_0 is the smallest intermolecular distance) that ensures an accuracy of the resonance shift values of about a few percents. To compare the theoretical values to the experimental ones we calculated the occupancy-weighted resonance frequency shift [solid line in Fig. 6(c)]. The agreement between theory and experiment is quite good. Because the disclike and spherelike molecules occupy different crystallographic positions, they are characterized by different values of the resonance frequency shift (Table III). For both kinds of molecules (''discs''and ''spheres''), the resonance frequency shift of the fundamental vibrations is mainly determined by the *isotropic* part of the intermolecular interaction. Furthermore, the repulsive interaction causes the most important contribution to these qualities. In case of the disclike molecules, the isotropic and anisotropic contributions due to the interaction between the nearest disclike molecules cancel each other out and the total resonance frequency shift is determined by the interaction with second (''spheres'') and subsequent neighbors. The ''sphere''-''disc'' interaction constitutes the majority of this quantity ($\approx$70%). This is the reason why the isotropic component dominates in the resonance frequency shift of γ-O_2.

TABLE III. Contribution of various components of the intermolecular interaction to the resonance frequency shift of the fundamental vibrations in the *y*-oxygen ($T=44$ K).

	Disclike molecules (cm^{-1})		
Type of interaction	Summation up to $R_{ij}=2R_0$	Nearest neighbors	Spherelike molecules (cm^{-1})
Isotropic part			
Dispersion	−0.377	−0.188	−0.326
Repulsion	1.823	1.017	1.543
Sum	1.446	0.829	1.217
Anisotropic part			
Dispersion	0.099	0.163	−0.102
Repulsion	−0.747	−0.978	0.461
Electrostatic	0.0078	0.0085	
Sum	−0.640	−0.807	0.359
Total resonance frequency shift	0.806	0.022	1.576

3. High-pressure behavior of vibron energy zone in solid nitrogen and oxygen

In case of the solid nitrogen, the available high-pressure data[41] are a natural extension of our results [Figs. 6(b) and 6(d)] over a high-density region. It is important to note that the environmental and resonance frequency shifts depend substantially differently upon pressure.[41] The former increases strongly with increasing pressure whereas the latter remains almost constant (~ 1 cm^{-1}) in α- and γ-N_2 ($T=4.2$ K). Consequently, the pressure behavior of the measured vibron frequencies at $\mathbf{k}=0$ (Raman frequencies) is mostly governed by the pressure-caused changes in the environmental frequency shift in these nitrogen phases.

Unfortunately, only frequencies of the vibron modes at $\mathbf{k}=0$ are known in high-pressure phases of oxygen.[55] The vibron frequency measured continuously increases due to pressure. Since the environmental and resonance shifts possess opposite signs and are characterized by comparable absolute values in orientationally ordered phases at ambient pressure [see Figs. 6(a) and 6(c)], a possible behavior of the vibron energy zone is not obvious increasing pressure.[56] To solve this problem based on experimental data, one needs to know the pressure dependence of the frequency of *single* molecule excitations ($\omega^s_{0\text{-}1}$) in addition to the available one[55] for the vibron frequency. To our knowledge, there is only one publication[14] concerning the absorption spectra of the phonon sideband of fundamental vibrations in low-pressure

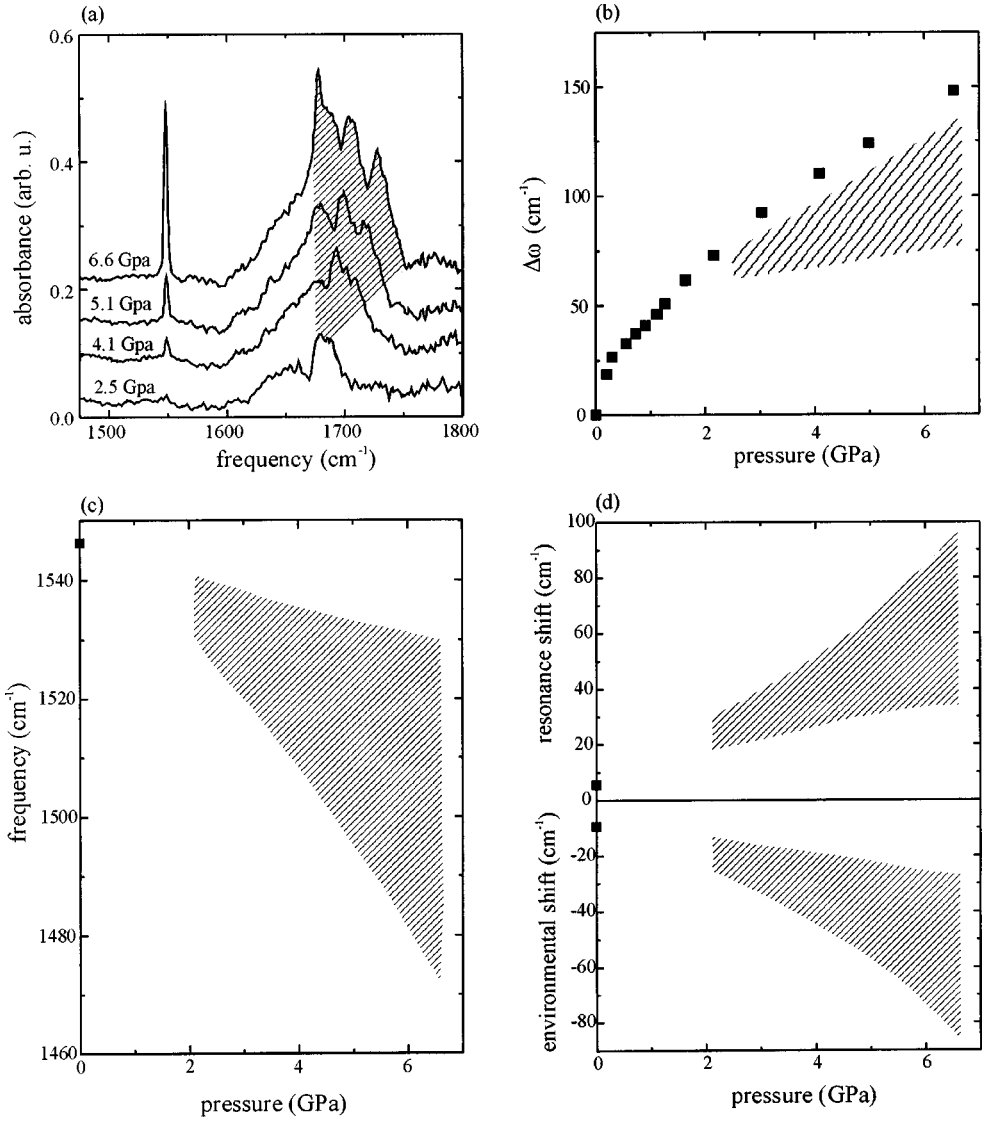

FIG. 7. (a) Evolution of the fundamental phonon sideband spectra of solid oxygen with pressure [Ref. 14(b), $T \approx 20$ K]. (b) Pressure-induced shift in frequency (solid oxygen, $T = 10-20$ K): filled quadrates—Raman high-frequency libron mode (Refs. 55, 57); shaded region—the region of the main singularity of the phonon sideband spectrum [of (a)]. (c) The ZPL frequency of the fundamental phonon sideband of solid oxygen as a function of pressure ($T = 10-20$ K): solid quadrate—our zero-pressure result, shaded region—the values deduced from (b) [Eq. 10(a)]. (d) Pressure induced changes in the environmental and resonance frequency shifts (solid oxygen, $T = 10-20$ K).

phases of solid oxygen ($p = 2.5-6.6$ GPa, $T = 23$ K). Unfortunately, only the Stokes part of the phonon sideband is clearly recognizable in these spectra [see Fig. 1 in Ref. 14(a)]. Consequently, we could not apply our procedure (Stokes/anti-Stokes deconvolution to find ZPL, Sec. III A) to determine the $\omega^s_{0\text{-}1}$ frequencies from these spectra. Hence, we used another approach to estimate the $\omega^s_{0\text{-}1}$ frequency values at high pressures. That is, we compared the pressure-caused frequency shift of singularities in spectra of the phonon sideband[14] $[\Delta\omega^{sb}_{sing}(p) = \omega^{sb}_{sing}(p) - \omega^{sb}_{sing}(p=0)]$ to the one of the libron modes[55,57] $[\Delta\omega_{lib}(p) = \omega_{lib}(p) - \omega_{lib}(p=0)]$. At this comparison, we used the fact that libron excitations are mainly responsible for main singularities in the phonon sideband spectra of α-O_2.[4,6,13]

Comparing the phonon sideband spectrum at 2.5 GPa [Fig. 7(a)] with the one at ambient pressure [Fig. 1(a), $T = 11.2$ K], one can easily recognize their principal similarity. The main maximum situated at 1683 ± 6 cm^{-1} at 2.5 GPa [Fig. 7(a)] corresponds to the main maximum of the phonon sideband spectrum at zero pressure $\omega^{sb}_{sing}(p=0) = 1617$ cm^{-1} [Fig. 1(a)], whereas other more weak maxima are smeared out in the high-pressure spectrum. The frequency of this main singularity is composed[13] of the ZPL frequency and the one of the high-frequency libron,

$$\omega^{sb}_{sing} \approx \omega^{s}_{0\text{-}1} + \omega^{hfr}_{lib}. \tag{10}$$

As pressure increases, the shape of the high-frequency part of the phonon sideband spectrum becomes more and more complicated [see Fig. 7(a)]. However, the region of possible position of this maximum can be obviously limited at $p > 4$ GPa [shown by a shaded sector in Fig. 7(a)]. The corresponding values of the $\Delta\omega^{sb}_{sing}(p)$ frequency shift are

shown by hatching in Fig. 7(b). It can be seen that this frequency region lies systematically lower than the frequency shift of the high-frequency libron mode [solid quadrates in Fig. 7(b), calculated by us from data[55,57]]. Moreover, the difference between these two quantities goes up with increasing pressure. Presuming that Eq. (10) holds at increasing pressure (at least semiquantitatively), we can paraphrase it in the form suitable for our analysis,

$$\omega^{s}_{0\text{-}1}(p) \approx \omega^{s}_{0\text{-}1}(p=0) + \Delta\omega^{\mathrm{sb}}_{\mathrm{sing}}(p) - \Delta\omega^{\mathrm{hfr}}_{\mathrm{lib}}(p). \quad (10a)$$

Introducing our $\omega^{s}_{0\text{-}1}$ value at zero pressure ($\approx$1547 cm^{-1}) as well as the $\Delta\omega^{\mathrm{hfr}}_{\mathrm{lib}}(p)$ and $\Delta\omega^{\mathrm{sb}}_{\mathrm{sing}}(p)$ frequency shift values [solid quadrates and shaded sector in Fig. 7(b), respectively] into Eq. (10a), we determined the region of possible values of the $\omega^{s}_{0\text{-}1}$ frequency of solid oxygen as a function of pressure at low temperature [shown by hatching in Fig. 7(c)]. Figure 7(c) shows that the band origin frequency ($\omega^{s}_{0\text{-}1}$) decreases as pressure increases (similarly to the one in the $^1\Delta_g$ excited electronic state[15]). Using the $\omega^{s}_{0\text{-}1}$ values obtained [Fig. 7(c)] together with the known[55] ones of the vibron frequency [$\omega^{\mathrm{vib}}_{0\text{-}1}(p)$], we deduced [Eqs. (6)] the environmental and resonance frequency shifts in solid oxygen as a function of pressure (up to 6.6 GPa) at low temperature [shown by shaded regions in Fig. 7(d)]. Despite some uncertainty of numerical values of these qualities at higher pressures [Fig. 7(d)], one can clearly recognize a general trend in their pressure behavior—the environmental frequency shift decreases whereas the resonance one rises with increasing pressure. That is, the fundamental vibron energy zone of solid oxygen broadens and its bottom and top move in opposite directions as pressure (density) increases. Therefore, the pressure-caused increase in the vibron frequency at $\mathbf{k}=0$ (the top of the vibron energy zone) observed experimentally[55] is explicitly caused by increasing the resonance frequency shift in solid oxygen [see Fig. 7(d)]. It is important to note that the vibron energy zone demonstrates qualitatively the same behavior as a function of density both in high-pressure [Fig. 7(d)] and in zero-pressure [Figs. 6(a) and 6(c)] regions despite these two sets of data being obtained by qualitatively different approaches. This generality of our results strongly supports the physical picture obtained. The qualitative explanation of such a behavior of the vibron energy zone in condensed phases of oxygen is already given by us in the previous paragraphs.

E. From spectra to the character of the orientational motion (β-nitrogen)

Since 1960, many efforts have been put by experimental and theoretical groups into obtaining a noncontradictory microscopic picture of a short-range orientational order in β-N_2 (see Ref. 16 for thorough discussion). However, it is not completed up to now. To describe a molecular motion in the azimuthal (φ) direction two qualitatively different models are used most: (i) noncorrelated (free) precession of all molecules[17(a),34] and (ii) the fixed mutual ($\varphi_i - \varphi_j$) orientation of 180° of neighboring (i, j) molecules accomplishing free jumps between six degenerate localized positions in hcp structure.[58] In this section we intend to use the resonance frequency shift in β-N_2 as a sensitive test to clarify this long-standing problem because this quality is mainly caused by correlations in orientational motion of nitrogen molecules (see Sec. III D 2). Hence, we calculated the anisotropic part of the resonance frequency shift for the different forms of the short-range orientational order in β-N_2. We used the intermolecular potential[59] as well as the structural data[34] at numerical calculations. For the sake of simplicity, we presupposed that the axes of nitrogen molecules are fixed at a certain polar angle relative to the c axis of hcp structure: $\vartheta_i = \vartheta_{\mathrm{prec}} = \arccos(\sqrt{1/3}) = 54.7°$ following the nuclear quadrupole resonance (NQR) data.[17(b)] At first, we checked the simplest possibility—the absence of any correlations in the azimuthal (φ) direction.[17(a),34] At this presumption, we obtained for the anisotropic component of the resonance frequency shift ($M^{\mathrm{anis}}_{0\text{-}1}$) a value of about $-0.03\ \mathrm{cm}^{-1}$ only. Consequently, a free precession must be ruled out and the mutual correlations in an azimuthal motion of molecules have to be taken in account in the β-N_2. Then, we analyzed the anisotropic part of the interaction between two nitrogen molecules [$U^{\mathrm{anis}}_{ij}(\mathbf{R}_{ij}, \theta_i, \theta_j, \varphi_i, \varphi_j)$], accomplishing a *correlated* precession, as a function of the relative azimuthal angle $\Delta\varphi_{ij} = \varphi_i - \varphi_j$ at arbitrary orientation of the vector $\mathbf{R}_{ij}$ connecting their centers of gravity,

$$\tilde{U}^{\mathrm{anis}}_{ij}(|\mathbf{R}_{ij}|, \mathbf{r}_{ij} = \mathbf{R}_{ij}/|\mathbf{R}_{ij}|, \Delta\varphi_{ij}) = 1/2\pi \int_0^{2\pi} U^{\mathrm{anis}}_{ij}(\mathbf{R}_{ij}, \vartheta_i, \vartheta_j, \varphi_i, \varphi_j)\big|_{\vartheta_i = \vartheta_j = \vartheta_{\mathrm{prec}}} d\varphi_i . \quad (11)$$

As expected, expression (11) does not depend on x and y components of the unit vector $\mathbf{r}_{ij}$ due to averaging over the φ angle of one molecule. However, it turns out that this function depends on the absolute value of the projection of the vector $\mathbf{r}_{ij}$ on the c axis. Therefore, it is different for pairs of molecules lying within one closed packed layer [Fig. 8(a)] and belonging to different layers [Fig. 8(b)]. The repulsive (dashed lines) and quadrupole-quadrupole (dash-dot lines) interactions are responsible for a general behavior of these potential functions. The minimum of the potential energy lies exactly at $\Delta\varphi^{\mathrm{adj.pl}}_{ij} = 180°$ for the pair of molecules belonging to adjacent layers whereas two minima exist for molecule pairs within basal planes: $\Delta\varphi^{\mathrm{bas.pl}}_{ij} \approx \pm 75°$. In the last case, the relative azimuthal angle of 180° corresponds to the *main* maximum of the potential function. Therefore, two kinds of molecular pairs exist in β-N_2. These results differ fundamentally from the *ad hoc* hypothesis by van der Avoird, Briels, and Jansen[58] who supposed the difference in the azimuthal angles of 180° for *every one* of pairs of molecules.

Introducing the $\tilde{U}^{\mathrm{anis}}_{ij}(|\mathbf{R}_{ij}|, \mathbf{r}_{ij} = \mathbf{R}_{ij}/|\mathbf{R}_{ij}|, \Delta\varphi_{ij})$ function into Eq. (3b), we calculated the anisotropic resonance frequency shift caused by both kinds of molecular pairs between the nearest neighbors in β-N_2—$M^{\mathrm{anis}}_{ij,\mathrm{bas.pl}}(\Delta\varphi_{ij})$ and $M^{\mathrm{anis}}_{ij,\mathrm{adj.pl}}(\Delta\varphi_{ij})$. These functions reproduce qualitatively the corresponding dependence of the potential energy upon the relative azimuthal angle between molecules (Fig. 8). For example, at $T = 36$ K, the $M^{\mathrm{anis}}_{ij,\mathrm{bas.pl}}(\Delta\varphi_{ij})$ quantity is $-0.062\ \mathrm{cm}^{-1}$ and $+0.09\ \mathrm{cm}^{-1}$ at the $\Delta\varphi_{ij}$ values corre-

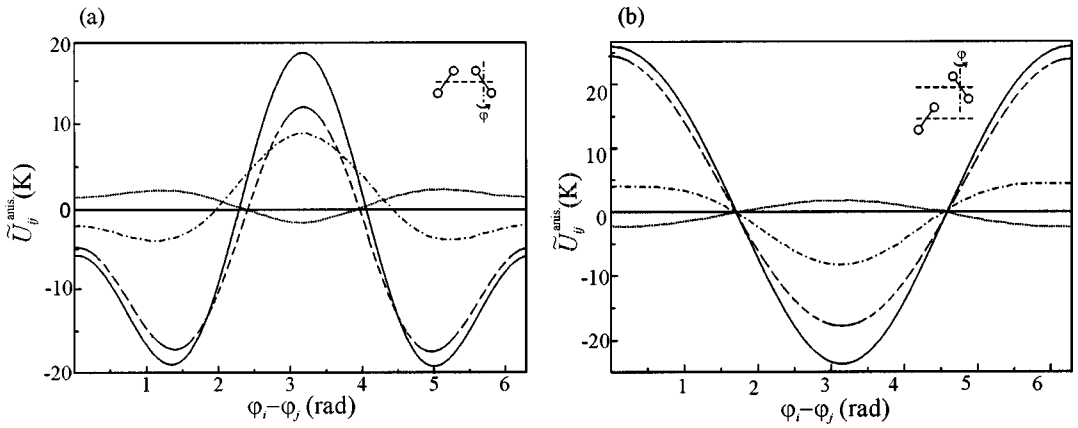

FIG. 8. Anisotropic part of the potential energy $[\tilde{U}_{ij}^{\text{anis}}(|\mathbf{R}_{ij}|,\mathbf{r}_{ij}=\mathbf{R}_{ij}/|\mathbf{R}_{ij}|,\Delta\varphi_{ij})$, Eq. (11)] of pairs of nitrogen molecules (solid lines) vs the mutual azimuthal angle $\Delta\varphi_{ij}=\varphi_i-\varphi_j$ at $\vartheta_i=\vartheta_j=\arccos(\sqrt{1/3})$ averaging over the azimuthal motion of one molecule [see Eq. (11)]: (a) nearest molecules within basal plane, (b) the ones from adjacent layers. The different constituents of this energy are shown by various kinds of lines: dotted—dispersion part, dashed—repulsive one, and dash-dot—quadrupole-quadrupole interaction.

sponding to the minimum ($\Delta\varphi_{\text{min}}^{\text{bas.pl}}\approx 75°$) and the maximum ($\Delta\varphi_{\text{max}}^{\text{bas.pl}}=180°$) of the potential energy, respectively. For a pair of molecules belonging to adjacent layers, similar values are: $M_{ij,\text{adj.pl}}^{\text{anis}}(\Delta\varphi_{\text{min}}^{\text{adj.pl}}=180°)=-0.145\ \text{cm}^{-1}$ and $M_{ij,\text{adj.pl}}^{\text{anis}}(\Delta\varphi_{\text{max}}^{\text{adj.pl}}=0)=+0.055\ \text{cm}^{-1}$. Therefore, the resonance frequency shift is very sensitive to the mutual orientation of nitrogen molecules. Using Eq. (3b) and taking into account the interaction between a central molecule ($i=0$) and its nearest neighbors ($j=1,...,12$) only, we can write the resonance frequency shift of the fundamental vibration in the β-N_2 as follows:

$$M_{0\text{-}1}(\mathbf{k}=0)=M_{0\text{-}1}^{\text{is}}(\mathbf{k}=0)+M_{\text{bas.pl}}^{\text{anis}}(\mathbf{k}=0)+M_{\text{adj.pl}}^{\text{anis}}(\mathbf{k}=0). \tag{12}$$

$M_{0\text{-}1}^{\text{is}}$ $(\mathbf{k}=0)\approx-0.12\ \text{cm}^{-1}$ (see Sec. III D 2); $M_{\text{bas.pl}}^{\text{anis}}$ $(\mathbf{k}=0)$ and $M_{\text{adj.pl}}^{\text{anis}}$ $(\mathbf{k}=0)$ are the components of the anisotropic parts of the resonance frequency shift caused by pairs of molecules within closed-packed layers and belonging to adjacent ones, respectively,

$$M_{\text{bas.pl}}^{\text{anis}}(\mathbf{k}=0)=6\int_0^{2\pi}M_{0i\text{bas.pl}}^{\text{anis}}(\Delta\varphi_{0i}^{\text{bas.pl}})\times\rho(\Delta\varphi_{0i}^{\text{bas.pl}})d(\Delta\varphi_{0i}^{\text{bas.pl}}), \tag{12a}$$

$$M_{\text{adj.pl}}^{\text{anis}}(\mathbf{k}=0)=6\int_0^{2\pi}M_{0i\text{adj.pl}}^{\text{anis}}(\Delta\varphi_{0i}^{\text{adj.pl}})\times\rho(\Delta\varphi_{0i}^{\text{adj.pl}})d(\Delta\varphi_{0i}^{\text{adj.pl}}), \tag{12b}$$

$\rho(\Delta\varphi_{0i})$ is a distribution function for the 0-i molecular pair dictated by the interaction between molecules over whole crystal and depending on temperature and lattice parameters. Since no long-range orientational order exists in the β-N_2 (''orientational liquid''), it is a very complex task to determine exactly the $\rho(\Delta\varphi_{0i})$ function. However, two limiting cases can be analyzed. First, if the relative azimuthal angles $\Delta\varphi_{0i}$ equal the values corresponding to the minimum of the pair potential function [Eq. (11)] for *any* pairs in Eqs. (12a,b), we obtain

$$M_{0\text{-}1}^{\text{up}}(\mathbf{k}=0)=M_{0\text{-}1}^{\text{is}}(\mathbf{k}=0)+6M_{0i,\text{bas.pl}}^{\text{anis}}(\Delta\varphi_{\text{min}}^{\text{bas.pl}})+6M_{0i,\text{adj.pl}}^{\text{anis}}(\Delta\varphi_{\text{min}}^{\text{adj.pl}}). \tag{13}$$

Of course, this case is not realistic but represents the uppermost estimate of the absolute value of the resonance frequency shift in β-N_2. Second case is related to a more realistic situation if only the pair correlations are important (so-called ''correlated orientational gas''), i.e.,

$$\rho(\Delta\varphi_{ij})\simeq\rho_{\text{pair}}(\Delta\varphi_{ij})\equiv\exp[-\tilde{U}_{ij}^{\text{anis}}(\Delta\varphi_{ij})/T]d(\Delta\varphi_{ij})\Big/\int_0^{2\pi}\exp[-\tilde{U}_{ij}^{\text{anis}}(\Delta\varphi_{ij})/T]d(\Delta\varphi_{ij}). \tag{14}$$

Then, Eqs. (12) are transformed to the form

$$M_{0\text{-}1}^{\text{low}}(\mathbf{k}=0)=M_{0\text{-}1}^{\text{is}}(\mathbf{k}=0)+6\left[\frac{\int M_{0/\text{bas.pl}}^{\text{anis}}(\Delta\varphi_{0i})\exp[-\tilde{U}_{0i}^{\text{bas.pl}}(\Delta\varphi_{0i}^{\text{bas.pl}})/T]d(\Delta\varphi_{0i}^{\text{bas.pl}})}{\int\exp[-\tilde{U}_{0i}^{\text{bas.pl}}(\Delta\varphi_{0i}^{\text{bas.pl}})/T]d(\Delta\varphi_{0i}^{\text{bas.pl}})}+\frac{\int M_{0i,\text{adj.pl}}^{\text{anis}}(\Delta\varphi_{0i})\exp[-\tilde{U}_{0i}^{\text{adj.pl}}(\Delta\varphi_{0i}^{\text{adj.pl}})/T]d(\Delta\varphi_{0i}^{\text{adj.pl}})}{\int\exp[-\tilde{U}_{0i}^{\text{adj.pl}}(\Delta\varphi_{0j}^{\text{adj.pl}})/T]d(\Delta\varphi_{0j}^{\text{adj.pl}})}\right]. \tag{15}$$

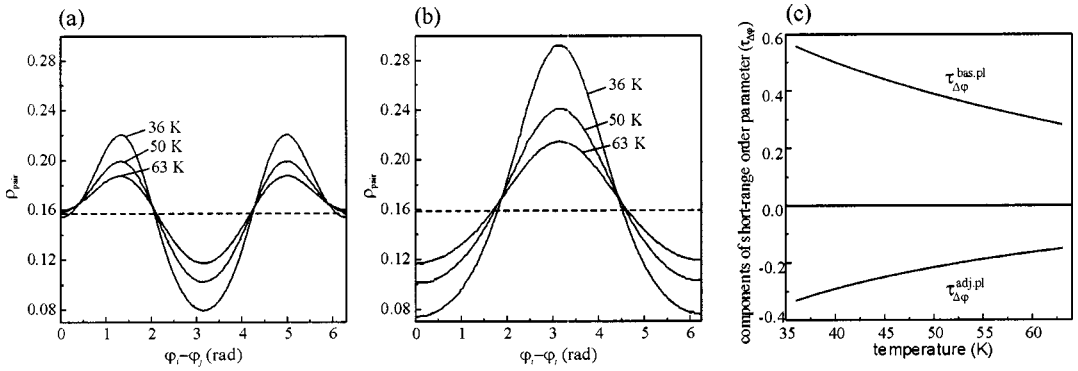

FIG. 9. (a), (b) Temperature evolution of the pair distribution function of the mutual orientation in the azimuthal direction [$\rho_{\text{pair}}(\Delta\varphi_{ij})$, Eq. (14)] for neighboring molecules in β-N_2 (solid lines): (a) within basal plane, (b) belonging to adjacent layers. The dashed lines correspond to free rotation. (c) Temperature dependence of the components of a two-component short-range order parameter describing the azimuthal motion of molecules in β-N_2 [Eqs. (16)].

This expression represents the lower estimate of the absolute value of the real resonance term.

The calculated resonance frequency shift values for these two cases are shown in Fig. 6(d) by dashed [Eq. (13)] and solid [Eq. (15)] lines, respectively. The experimental points (quadrates) are situated between these two limiting curves as expected. These results verify our theoretical model. Obviously, the difference between the theoretical (solid line) and experimental values can be attributed to many-particle correlations in the azimuthal motion of molecules.

An existence of two different kinds of molecule pairs possessing different mutual orientations means that an azimuthal motion of nitrogen molecules is actually described by a two-component short-range order parameter [$\tau^{\text{sh.ord}}_{\Delta\varphi} \cong \{\tau^{\text{bas.pl}}_{\Delta\varphi}, \tau^{\text{adj.pl}}_{\Delta\varphi}\}$] in β-N_2 whose components are related to two different distribution functions of mutual orientations of molecules—$\rho(\Delta\varphi^{\text{bas.pl}}_{0j})$ and $\rho(\Delta\varphi^{\text{adj.pl}}_{0j})$. Using the expressions (14) as an estimate of these functions, we calculated those at different temperatures [Figs. 9(a) and 9(b)]. At $T=0$, $\rho_{\text{pair}}(\Delta\varphi^{\text{bas.pl}}_{0j})$ and $\rho_{\text{pair}}(\Delta\varphi^{\text{adj.pl}}_{0j})$ are equal to 0.5 and 1, respectively, at mutual orientations corresponding to minima ($\Delta\varphi^{\text{bas.pl}}_{0}, \Delta\varphi^{\text{adj.pl}}_{0}$) of the pair potential function [Eq. (11)] and to zero at any other angles [see Eq. (14)]. The quantity of 0.5 reflects an existence of two equiprobable mutual orientations for molecular pairs within closed-packed layers [see Fig. 8(a)]. As temperature increases, both distribution functions approach $\rho_{\text{rot}}(\Delta\varphi_{ij}) \equiv 1/2\pi \approx 0.159$ (free rotation). However, up to the melting point nitrogen molecules possess the preferable mutual orientation being different for two kinds of molecular pairs [Figs. 9(a) and 9(b)]. To characterize the extent to which the mutual orientation of molecules is fixed at $\Delta\varphi^{\text{bas.pl}}_{0}$ and $\Delta\varphi^{\text{adj.pl}}_{0}$ positions, we designed the components of a short-range order parameter as follows:

$$\tau^{\text{bas.pl}}_{\Delta p}(T) = \frac{1}{\left|\cos(\Delta\varphi^{\text{bas.pl}}_{0})\right|}\int_0^{2\pi}\cos(\Delta\varphi^{\text{bas.pl}}_{0i}) \times \rho_{\text{pair}}(T,\Delta\varphi^{\text{bas.pl}}_{ij})d(\Delta\varphi^{\text{bas.pl}}_{0i}), \qquad (16a)$$

$$\tau^{\text{adj.pl}}_{\Delta\varphi}(T) = \frac{1}{\left|\cos(\Delta\varphi^{\text{adj.pl}}_{0})\right|}\int_0^{2\pi}\cos(\Delta\varphi^{\text{adj.pl}}_{0i}) \times \rho_{\text{pair}}(T,\Delta\varphi^{\text{adj.pl}}_{ij})d(\Delta\varphi^{\text{adj.pl}}_{0i}), \qquad (16b)$$

$\Delta\varphi^{\text{bas.pl}}_{0}$ is slightly changed from $\pm 75.36°$ at 36 K to ± 74.85 at 63 K due to thermal expansion while $\Delta\varphi^{\text{adj.pl}}_{0}$ equals 180° for any intermolecular distance. The values of $\tau^{\text{bas.pl}}_{\Delta\varphi}(T)$ and $\tau^{\text{adj.pl}}_{\Delta\varphi}(T)$ equal 1 and -1, respectively, at $T=0$ and approach zero as $T\to\infty$. Obviously, the decrease in absolute values of both components of the short-range order parameter [Fig. 9(c)] is caused by the temperature changes in the corresponding distribution functions [Figs. 9(a), 9(b)]. However, additional important information can be easily drawn from Fig. 9(c). The absolute values of $\tau^{\text{bas.pl}}_{\Delta\varphi}(T)$ are about two times larger then the $\tau^{\text{adj.pl}}_{\Delta\varphi}(T)$ one. That is, an azimuthal motion of molecules in hcp structure of β-N_2 is substantially stronger correlated for neighboring molecules within basal plane compared to the one belonging to adjacent layers. Since any drastic changes in the resonance frequency shift values [Fig. 6(d)] as well as in short-range translational orde[18(b)] do not occur by melting nitrogen crystal, we believe a similar character of a short-range orientational order is preserved in liquid nitrogen.

IV. CONCLUSION

The phonon sidebands to fundamental and first overtone internal vibrations were systematically investigated by Fourier transform infrared spectroscopy in all condensed phases of nitrogen and oxygen at ambient pressure as a function of temperature (from 10 K to the boiling points). Due to an improved growing technique, we were able to grow thick crystal samples (thickness up to 20 mm) with an excellent optical quality. As a result, we determined an exact complete profile of the whole phonon sideband consisting of Stokes and anti-Stokes parts. High-accuracy data on vibron frequencies were also collected by Raman spectroscopy in solid and liquid oxygen for comparison to ir data.

Dividing the experimental phonon sideband profile into Stokes and anti-Stokes components, we determined the band

origin frequency (as ZPL) and explored its temperature behavior in both substances investigated. We showed that the ZPL frequencies differ significantly from the vibron ones in both nitrogen and oxygen. Based on our analysis of the phonon sidebands to the first overtone as well as on available literature data, we present a series of direct experimental proofs that the ZPL frequency corresponds to the frequency of the fundamental vibrations of *single* molecules in a condensed medium. We interpret this basic result as a strong evidence for the fact that an ir-active phonon sideband to internal vibrations is caused by an interaction between lattice excitations and internal vibrations of *single* molecules in molecular solids. Since we obtained similar results for the phonon sidebands to electronic and electronic-vibrational excitations, we believe that this conclusion possesses a general character for in-active phonon sidebands to any kinds of internal molecular excitations.

A joint analysis of the Raman (vibron frequencies) and ir (ZPL frequency) data allowed us to characterize the fundamental vibron energy zones of both substances quantitatively and to explore their temperature behavior in a wide temperature range (from 10 K to boiling points). The vibron excitations are described by a negative effective mass in all oxygen phases and a positive one in β-nitrogen and liquid nitrogen according to our results. Our own analysis of high-pressure spectroscopic data by others revealed that the increase in Raman frequencies of vibron excitations of solid oxygen by pressure is mainly caused by broadening its vibron energy zone due to pressure.

We also presented a theoretical analysis of the resonance frequency shift of the fundamental vibrations in orientationally disordered phases of nitrogen (β-N_2) and oxygen (γ-O_2), consistent with our spectroscopic results. We showed that the resonance frequency shift is mostly caused by the isotropic part of the intermolecular interaction in γ-O_2 and by the anisotropic one in β-N_2. Based on this analysis, we found for β-N_2 that an azimuthal orientational motion of molecules along the *c* axes of hcp structure is strongly correlated. The type of these correlations is substantially different for neighboring molecules within closed-packed layers and belonging to adjacent ones: the former are preferably oriented at the mutual azimuthal angle of about $\pm 75°$ while the latter—at the one of 180°.

ACKNOWLEDGMENT

This work was supported by Deutsche Forschungsgemeinschaft (Grants Nos. Jo 86/10-1 and Jo 86/11-1).

[1] (a) M. L. Oxholm and D. Williams, Phys. Rev. **76**, 151 (1949); (b) A. L. Smith, W. E. Keller, and H. L. Johnston, *ibid.* **79**, 728 (1950).

[2] B. R. Cairns and G. C. Pimentel, J. Chem. Phys. **43**, 3432 (1965).

[3] H. J. Jodl, H. W. Loewen, and D. Griffith, Solid State Commun. **61**, 503 (1987).

[4] H. W. Löwen, K. D. Bier, and H. J. Jodl, J. Chem. Phys. **93**, 8565 (1990).

[5] G. Cardini, R. Righini, H. W. Löwen, and H. J. Jodl, J. Chem. Phys. **96**, 5703 (1992).

[6] M. Minenko, M. Vetter, A. P. Brodyanski, and H. J. Jodl, Fiz. Nizk. Temp. **26**, 947 2000 [Sov. J. Low Temp. Phys. **26**, 699 (2000)].

[7] R. M. Hochstrasser and P. N. Prasad, J. Chem. Phys. **56**, 2814 (1972).

[8] A. S. Davydov, *Theory of Molecular Excitons* (Plenum, New York, 1971), English translation by B. Dresner.

[9] G. Zumofen and K. Dressler, J. Chem. Phys. **64**, 5198 (1976); G. Zumofen, *ibid.* **68**, 3747 (1978).

[10] P. L. Kunsch, J. Chem. Phys. **70**, 1343 (1979).

[11] H. W. Löwen, K. D. Bier, H. J. Jodl, A. Löwenschuss, and A. Givan, J. Chem. Phys. **90**, 5309 (1989).

[12] L. H. Jones, S. F. Agnew, B. I. Swanson, and S. A. Ekberg, J. Chem. Phys. **85**, 428 (1986).

[13] S. A. Medvedev, A. P. Brodyanski, and H. J. Jodl, Phys. Rev. B **63**, 184302 (2001).

[14] (a) F. A. Gorelli, L. Ulivi, M. Santoro, and R. Bini, Phys. Rev. B **60**, 6179 (1999); (b) F. A. Gorelli, Ph.D. thesis, dell' Universita di Firenze, 2000.

[15] A. Brodyanski, S. Medvedev, M. Minenko, and H. J. Jodl, in *Frontiers of High-Pressure Research II: Application of High Pressure to Low-Dimensional Novel Electronic Materials*, Vol. 48 of *NATO Science Series II: Mathematics, Physics and Chemistry*, edited by H. D. Hochheimer, B. Kuchta, P. K. Dorhout, and J. L. Yarger (Kluwer Academic, Dordrecht, 2001), pp. 217–234.

[16] *Physics of Cryocrystals*, edited by V. G. Manzhelii and Yu. A. Freiman (AIP, Woodbury, New York, 1997).

[17] (a) W. E. Streib, T. H. Jordan, and W. N. Lipscomb, J. Chem. Phys. **37**, 2962 (1962); T. H. Jordan, H. W. Smith, W. E. Streib, and W. N. Lipscomb, *ibid.* **41**, 756 (1964); (b) A. S. De Reggi, P. C-Capera, and T. A. Scott, J. Magn. Reson. (1969-1992) **1**, 144 (1969).

[18] (a) *Physics of Simple Liquids*, edited by H. N. V. Temperley, J. S. Rowlinson, and G. S. Rushbrooke, (North-Holland, Amsterdam, 1968); (b) A. P. Brodyanskii and Yu. A. Freiman, Fiz. Nizk. Temp. **12**, 1212; 1986 [Sov. J. Low Temp. Phys. **12**, 684 (1986)].

[19] I. N. Krupskii, A. I. Prokhvatilov, Yu. A. Freiman, and A. I. Erenburg, Fiz. Nizk. Temp. **5**, 271 1979 [Sov. J. Low Temp. Phys. **5**, 130 (1979)].

[20] A. P. Brodyanskii and Yu. A. Freiman, Fiz. Nizk. Temp. **11**, 994 1985 [Sov. J. Low Temp. Phys. **11**, 549 (1985)].

[21] (a) R. A. Alikhanov, Zh. Exp. Teor. Fiz., Pis'ma Red. **5**, 430 1967 [JETP Lett. **5**, 349 (1967)] (b) R. J. Meier and R. B. Helmholdt, Phys. Rev. B **29**, 1387 (1984).

[22] F. Dunstetter, O. Hardouin Duparc, V. P. Plakhty, J. Schweizer, and A. Delapalme, Fiz. Nizk. Temp. **22**, 140, 1996 [Sov. J. Low Temp. Phys. **22**, 101 (1996)].

[23] A. A. Chernov, *Modern Crystallography III: Crystal Growth*, Springer Series in Solid-State Sciences Vol. 36 (Springer Verlag, Berlin, 1984).

[24] J. Xie, M. Enderle, K. Knorr, and H. J. Jodl, Phys. Rev. B **55**, 8194 (1997).
[25] R. D. Beck, M. F. Hineman, and J. W. Nibler, J. Chem. Phys. **92**, 7068 (1990).
[26] (a) R. D. Etters, K. Kobashi, and J. Belak, Phys. Rev. B **32**, 4097 (1985); (b) A. Helmy, K. Kobashi, and R. D. Etters, J. Chem. Phys. **80**, 2782 (1984); *ibid.* **82**, 4731 (1985).
[27] L. Jin and K. Knorr, Phys. Rev. B **47**, 14 142 (1993).
[28] J. K. Kjems and G. Dolling, Phys. Rev. B **11**, 1639 (1975).
[29] F. D. Medina and W. B. Daniels, J. Chem. Phys. **64**, 150 (1976).
[30] V. M. Loktev (private communication).
[31] M. Vetter, M. Jordan, A. P. Brodyanski, and H. J. Jodl, J. Phys. Chem. A **104**, 3698 (2000).
[32] (a) I. Suzuki, J. Mol. Spectrosc. **25**, 479 (1968); (b) K. P. Huber and G. Herzberg, *Molecular Spectra and Molecular Structure. IV. Constants of Diatomic Molecules* (Van Nostrand Reinhold Company, New York, 1979).
[33] For example, the shape of the nitrogen phonon sideband to internal vibrations of the CO impurity is very similar to the one of the matrix molecules (compare Figs. 1 and 7 in Ref. 27).
[34] I. N. Krupskii, A. I. Prokhvatilov, and A. I. Erenburg, Fiz. Nizk. Temp. **1**, 359 1975 [Sov. J. Low Temp. Phys. **1**, 178 (1975)].
[35] (a) J. Van Kranendonk, Physica (Amsterdam) **24**, 347 (1958); (b) F. N. Hooge and J. A. A. Ketelaar, *ibid.* **23**, 423 (1957); J. P. Colpa and J. A. A. Ketelaar, *ibid.* **24**, 1035 (1958).
[36] D. A. Hatzenbuhler and L. Andrews, J. Chem. Phys. **56**, 3398 (1972).
[37] The fundamental frequency of the single $^{14}N_2$ molecules [$\omega^s_{0\text{-}1}(^{14}N_2) = 2328.48\ \mathrm{cm}^{-1}$] was reconstructed by us from the one of the $^{15}N\,^{14}N$ isotope (0.74%) in the α^{14}-N_2 crystal ($\omega^s_{0\text{-}1}(^{15}N^{14}N) = 2289.928 \pm 0.007\ \mathrm{cm}^{-1}$, Ref. 38) using an obvious relation between the fundamental frequencies of different isotopes matrix isolated in the same medium: $\omega^s_{0\text{-}1}(^{14}N_2) = \omega^{\mathrm{gas}}_{0\text{-}1}(^{14}N_2) + [(B_e/\omega_e)_{^{14}N_2}/(B_e/\omega_e)_{^{15}N\,^{14}N}][\omega^s_{0\text{-}1}(^{15}N\,^{14}N) - \omega^{\mathrm{gas}}_{0\text{-}1}(^{15}N\,^{14}N)]$. Here $\omega^{\mathrm{gas}}_{0\text{-}1}$ is the frequency of the 0-1 internal vibrational transition in the free molecule, B_e and ω_e are the rotational and harmonic vibrational constants, respectively.
[38] R. Beck and J. W. Nibler, Chem. Phys. Lett. **159**, 79 (1989).
[39] I. I. Abram, R. M. Hochstrasser, J. E. Kohl, M. G. Semack, and D. White, J. Chem. Phys. **71**, 153 (1979).
[40] K. K. Rebane, *Impurity Spectra of Solids* (Plenum, New York, 1970).
[41] M. M. Thiery and V. Chandrasekharan, J. Chem. Phys. **67**, 3659 (1977).
[42] (a) A. D. Buckingham, Proc. R. Soc. London, Ser. A **248**, 169 (1958); Faraday Soc. Trans. **56**, 26 (1960); (b) J. Van Kranendonk, *Solid Hydrogen* (Plenum, New York, 1983).
[43] S. Flügge, P. Walger, and A. Weiguny, J. Mol. Spectrosc. **23**, 243 (1967).
[44] L. Infeld and T. E. Hull, Rev. Mod. Phys. **23**, 21 (1951).
[45] G. Herzberg, *Molecular Spectra and Molecular Structure I. Spectra of Diatomic Molecules* (Van Nostrand Reinhold Company, New York, 1950).
[46] W. M. Grundy, B. Schmitt, and E. Quirico, Icarus **105**, 254 (1993).
[47] N. Legay-Sommaire and F. Legay, Chem. Phys. **66**, 315 (1982).
[48] The authors of Ref. 46 erroneously assigned the *whole* spectrum of the β-nitrogen and liquid nitrogen in this spectral region to the second physical mechanism.
[49] F. Legay and N. Legay-Sommaire, Chem. Phys. **206**, 363 (1996).
[50] D. Keutel, F. Siefert, K.-L. Oehme, A. Asenbaum, and M. Musso, Phys. Rev. Lett. **85**, 3850 (2000).
[51] B. Oksengorn, D. Fabre, B. Lavorel, R. Saint-Loup, and H. Berger, J. Chem. Phys. **94**, 1774 (1991).
[52] The relatively small quadrupole-quadrupole term possesses the dependence on density ($\sim R^{-5}$) similar to the dispersion term ($\sim R^{-6}$) and, consequently, does not affect our considerations.
[53] J. De Kinder, E. Goovaerts, A. Bouwen, and D. Schoemaker, Phys. Rev. B **42**, 5953 (1990).
[54] P. Piecuch, A. E. Kondo, V. Spirko, J. Chem. Phys. **104**, 4699 (1996).
[55] H. J. Jodl, F. Bolduan, and H. D. Hochheimer, Phys. Rev. B **31**, 7376 (1985).
[56] In the theoretical calculations carried out in Ref. 26, *only* the environmental frequency shift was considered, analyzing the pressure-caused shift of the vibron frequency of solid oxygen.
[57] Y. Mita, M. Kobayashi, and S. Endo, Phys. Rev. B **62**, 8891 (2000).
[58] A. van der Avoird, W. J. Briels, and A. P. J. Jansen, J. Chem. Phys. **81**, 3658 (1984).
[59] A. Mulder, J. P. L. Michels, and J. A. Schouten, J. Chem. Phys. **105**, 3235 (1996).